Macromolecules

pubs.acs.org/Macromolecules Article

Structure–Property Relationships of Self-Healing Polymer Networks Based on Reversible Diels–Alder Chemistry

Seppe Terryn,* Joost Brancart, Ellen Roels, Robrecht Verhelle, Ali Safaei, Audrey Cuvellier, Bram Vanderborght, and Guy Van Assche

Cite This: *Macromolecules* 2022, 55, 5497–5513 Read Online

ACCESS | Metrics & More | Article Recommendations | Supporting Information

Downloaded via UNIV OF CAMBRIDGE on November 3, 2022 at 16:09:27 (UTC).
See https://pubs.acs.org/sharingguidelines for options on how to legitimately share published articles.

ABSTRACT: Recently, the Diels–Alder reaction between furan and maleimide functional groups has been exploited in dynamic reversible covalent networks, introducing a healing ability and reprocessing in various applications. Both applications and (re)processing techniques impose specific requirements, which can be met by the large tunability of the material properties of Diels–Alder-based networks. The extensive set of structure–property relations presented in this paper allows for designing Diels–Alder networks meeting a broad range of material properties. Three major network design parameters are defined that influence these properties: the Diels–Alder concentration, the degree of functionality of the reactive maleimide and furan groups on the monomers, and the stoichiometric ratio between these reactive groups. Their individual influences on the kinetics and the thermomechanical, rheological, and healing properties were investigated via tensile testing, differential scanning calorimetry, dynamic mechanical analysis, and dynamic rheometry. By tuning the design parameters independently, mechanical properties can be matched with requirements imposed by applications by changing the Diels–Alder concentration, while healing speeds can be further altered by the stoichiometric ratio between maleimide and furan groups. In addition, the temperature of gelation, crucial for processing, can be tuned by means of the functionality parameter, meeting requirements imposed by manufacturing techniques.

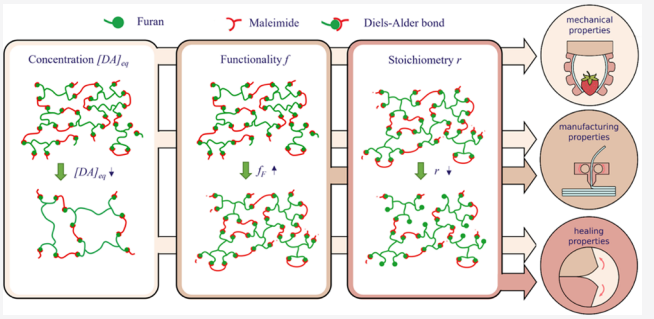

INTRODUCTION

Reversible covalent chemistries have been used to combine high strength and stability with healing capacity[1] and reprocessability,[2] able to heal microscopic and macroscopic damage. In this category, the Diels–Alder (DA) reaction, described by Otto Diels and Kurt Alder,[3] is one of the most widely used thermoreversible equilibrium reactions for constructing reversible covalent polymeric networks with intrinsic self-healing abilities. In most cases, the cycloaddition of furan, a conjugated electron-rich diene, and maleimide, an electron-poor dienophile, is used to form DA cycloadducts.[4] These materials were first developed as coatings for the corrosion protection of metals.[5,6] Later, these reversible networks were adopted to fabricate complex three-dimensional components, like healable soft robots,[7] that are able to recover their material properties and functional performance after being cut into two pieces. This has sparked the innovation of intrinsic self-healing materials for structural applications, putting more stringent requirements on these self-healing materials, spurring major advancements in both the self-healing materials and robotics field, as well as in additive manufacturing.[8]

The bodies of soft robots, an emerging type of robots, are biologically inspired and consist, for a large part, of soft material, mostly flexible polymers, or fabric materials.[9] Because of their inherent softness, these robots provide safe human–robot interactions, can produce large deformations, and are adaptable, making them suitable for soft gripper applications[10] for food manipulators,[11] prosthesis,[12] social robots,[13] surgical tools,[14] and robotic co-workers.[13] However, this softness comes at a price, as the components are vulnerable to different damaging modes like cuts, punctures, and tears due to sharp objects, as well as fatigue and interfacial debonding. Recent works[7] demonstrate that manufacturing the flexible bodies of soft robots out of self-healing polymers enables healing of damage with sizes ranging up to the centimeter scale. In contrast to coating applications, in soft robotics, intrinsic self-healing polymers make up structural 3D components, requiring excellent mechanical strength and stability, as well as elastomeric behavior.[15,16] Although a large variety of self-healing mechanisms are exploited in soft robotics,[7] including

Received: March 1, 2022
Revised: May 25, 2022
Published: June 25, 2022

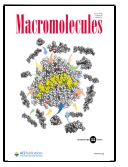

ACS Publications © 2022 American Chemical Society

https://doi.org/10.1021/acs.macromol.2c00434
Macromolecules 2022, 55, 5497–5513

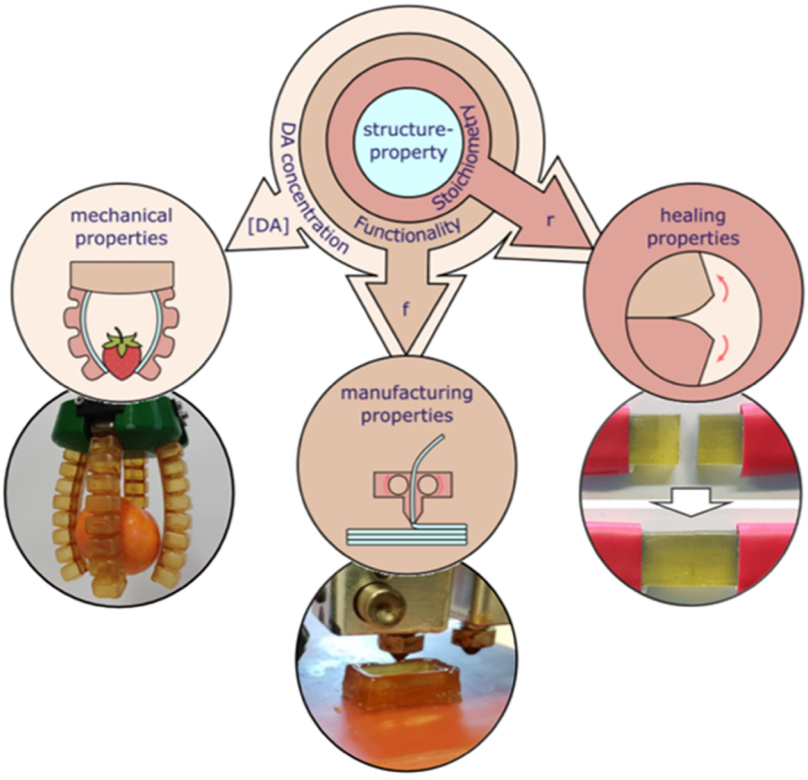

Figure 1. Based on the literature, three main network design parameters were defined, including the Diels–Alder concentration [DA], the functionality *f*, and the stoichiometric ratio *r*. By independently tuning these network design parameters, the material properties can be altered to fit mechanical and healing kinetic requirements imposed by the application (*e.g.*, soft robotics[20]) and rheological properties to fit processing and manufacturing requirements (*e.g.*, for 3D printing[31]).

different extrinsic,[17] supramolecular,[18] and dynamic covalent mechanisms,[19] the DA reversible chemistry was the first to be used in healable soft robots.[20]

In soft robotics, elastomers are used with mechanical properties varying over a broad range, e.g., the Young's modulus varies from 10^3 to 10^7 Pa,[21] and often materials with divergent properties are combined in a single part to generate complex anisotropic motions, with specific stiffnesses or differences in stiffness being essential to generate a passive intelligent behavior[22] or complex actuation modes.[23] To meet the demands imposed by applications like soft robotics, the mechanical properties of the intrinsic self-healing materials have to be tunable over a broad range. As reported in a previous study,[24] the mechanical properties of DA networks can be tuned via the crosslink density, which itself depends on the DA concentration in the network, influenced by the molar mass per DA functional group of the monomer units,[24] as well as the molar ratio between them.[25−28]

This Diels–Alder concentration also influences the thermomechanical properties, including the viscoelastic behavior at different temperatures. Higher Diels–Alder concentrations push the glass transition and gel transition to higher temperatures.[29] The latter transition is highly influenced by the monomer functionality as well, as illustrated by Li et al.[30] Consequently, the monomer functionality highly influences the rheological behavior, and with extension the manufacturing of the thermoreversible networks. For fused filament fabrication, which is an additive manufacturing technique, the gel transition of the DA networks was pushed to higher temperatures using furan compounds having a higher furan degree of functionality.[31] This speeds up the reaction kinetics during printing, leading to faster solidification and enhancing both print speed and resolution.

Although a higher crosslink density leads to an increase in the reaction rate,[25] it is not translated into improved healing rates, due to the reduction of mobility caused by the additional crosslinks. Alternatively, the stoichiometric ratio between the reactive maleimide and furan functional groups has been exploited by the authors to greatly improve the healing rate, increasing both the reaction kinetics and the network mobility.[28] A low maleimide-to-furan ratio, achieved through introducing an excess of furan reactive groups in the network, leads to an increase in reaction kinetics of the DA reaction.[32] The faster reaction kinetics allow healing under ambient conditions, as demonstrated for a pneumatic soft robotic gripper,[33] manufactured from a DA elastomeric network with a low stoichiometric ratio. This eliminates the need for an external heat stimulus and makes these DA networks truly autonomous self-healing materials.

Based on the literature, we define three main network design parameters that influence the material properties: the DA concentration at 25 °C, the monomer functionality, and the stoichiometric ratio between the reactive groups. In most research papers, these network design parameters are not varied independently; typically several parameters are changed simultaneously. As such, relations describing the direct effect of these design parameters on the material properties are largely lacking. In this paper, we made special efforts to independently change the network design parameters, while keeping the others constant, to investigate their effect on the thermomechanical and viscoelastic behavior and on the reaction kinetics (Figure 1). We will illustrate that by tuning the network design

https://doi.org/10.1021/acs.macromol.2c00434
Macromolecules 2022, 55, 5497−5513

parameters independently, mechanical and viscoelastic properties can be matched with the requirements imposed by the application by changing the crosslink density, largely controlled by the concentration of adducts formed, [DA], while the healing rate can be altered by the maleimide-to-furan stoichiometric ratio r. In addition, the temperature of the reversible gel transition can be tuned by means of the functionality of reactive groups f of the monomers used, to meet requirements imposed by the processing and/or manufacturing techniques.

RESULTS

Network Design Parameters. In this work, elastomeric networks are formed by crosslinking through the DA cycloaddition reaction between furan (diene) and maleimide (dienophile) (Figure 2). The maleimide group is present on a bismaleimide (DPBM), while the furan group is located on a furan-functionalized Jeffamine (FFJ), created by an irreversible epoxy-amine reaction between furfuryl glycidyl ether and the amino groups of the Jeffamine (Figure 3 and details in the Experimental Section and Supporting Information 2 and 3). The synthesized elastomeric network is thermoreversible. As the adduct formation is exothermic, upon heating the network, the crosslink density will decrease as the DA reaction equilibrium shifts toward the formation of reactive furan and maleimide groups (in endothermic sense). Consequently, both the number of reactive functional groups and the molecular mobility in the solid network increase, which allows performing the healing at typical temperatures of 80−90 °C.[20,26,34] Further increasing the temperature leads to degelation. This occurs at the gel-transition temperature T_{gel}, when the conversion drops below the gel conversion and the material loses its network structure, as it breaks down into a viscous liquid polymer. This gel transition is completely reversible, as upon cooling the DA reaction occurs, the concentration of DA bonds increases, and the material gels at T_{gel}. Upon cooling, the crosslink density in this reformed network increases and the initial properties at room temperature are eventually completely regained.

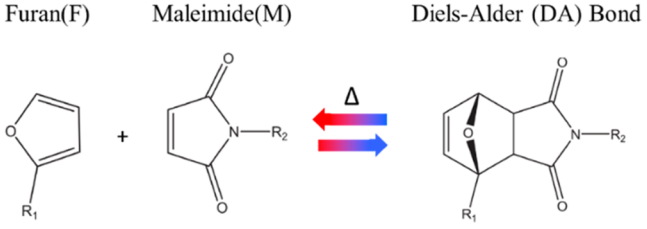

Figure 2. DA cycloaddition is an equilibrium reaction between furan and maleimide, which form DA adducts. The equilibrium is temperature-dependent: upon increasing/decreasing the temperature, the equilibrium shifts to the left/right, increasing/decreasing the fraction of unbound maleimide and furan.

To investigate the relations between the network structure and the material properties, a large variety of 10 elastomeric networks was created, differing in the type of monomers used in the synthesis and/or the ratio between them. Figure 4 illustrates the three network design parameters considered for the DA polymer networks presented in this work: (i) the DA concentration $[DA]_{eq}$ at the application temperature (room temperature), (ii) the functionality f of reactive groups on the monomers, and (iii) the stoichiometric ratio r between initial maleimide and furan active groups.

These three design parameters allow synthesizing a wide variety of DA networks with distinctly different properties. The knowledge of the direct effect of these network design parameters on the thermal properties and transitions allows for the design and preparation of reversible polymer network materials with customized thermomechanical and thermoresponsive properties for dedicated applications. These applications include self-healing coatings,[64] soft robotic actuators,[20,26,34] and advanced polymer processing.[8,35,36] In the following sections, these design parameters and their effect on the material properties will be consecutively addressed. However, first, the mechanistic kinetic model of the DA equilibrium reaction is introduced. Besides these three, other design parameters exist, including the type of Diels−Alder bonds, that influences the reactivity, and the flexibility of the building block. The study of the effect of these parameters is out of the scope of this work because it requires designing new syntheses.

Diels−Alder Kinetics. As extensively described in our previous work[32] and by Froidevaux et al.,[37] during the Diels−Alder (DA) reaction of furan (F) with maleimide (M), two stereoisomeric DA adducts are formed: the kinetically favored endo isomer and the thermodynamically more stable exo isomer. This implies that the kinetics of the complete DA reaction can be described by the two forward and two reverse DA (rDA) reactions of the endo and exo stereoisomers and the

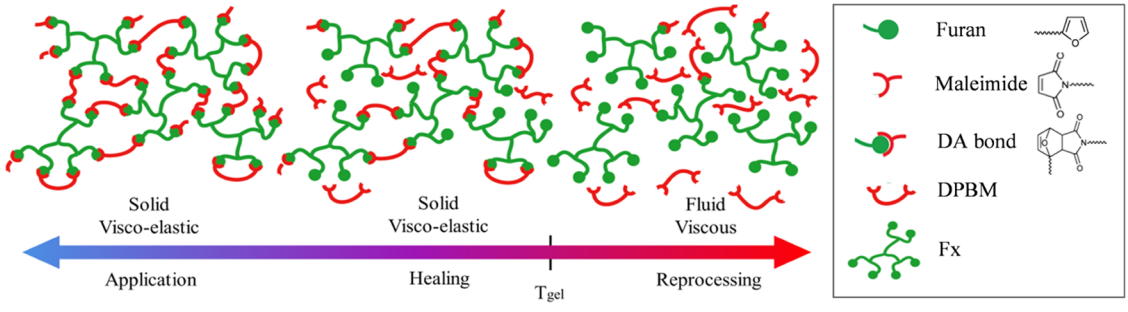

Figure 3. Elastomeric networks are created by reversible DA crosslinks formed by an equilibrium reaction between maleimide- and furan-functionalized molecules. The resulting network is thermoreversible. Upon heating the polymer, the equilibrium in the DA reaction shifts toward the unbound state, decreasing the number of DA bonds and increasing the number of furan and maleimide units, increasing the reactivity as well as mobility in the network. At the gel-transition temperature (T_{gel}), extensive debonding leads to degelation of the network into a viscous polymer. Upon cooling, the reversible network is reformed and a solid network polymer is recreated.

https://doi.org/10.1021/acs.macromol.2c00434
Macromolecules 2022, 55, 5497−5513

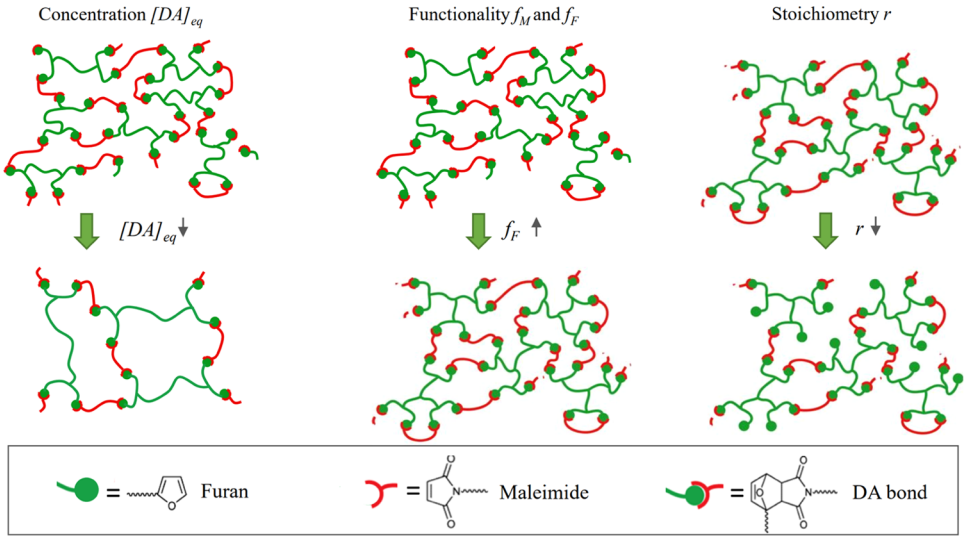

Figure 4. Three network design parameters that allow us to synthesize a wide variety of DA polymers with varying thermomechanical and physicochemical behavior: equilibrium DA concentration $[DA]_{eq}$; furan and maleimide functionalities f_F and f_M, respectively; and stoichiometry r.

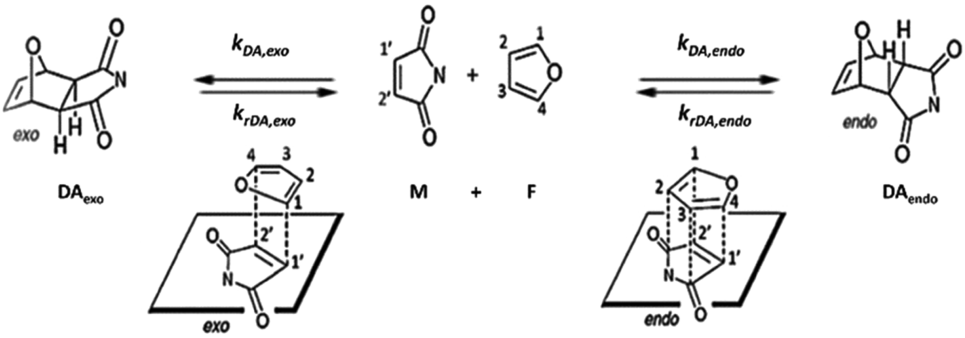

Figure 5. Reversible Diels–Alder reaction is an equilibrium reaction between furan groups (F), acting as the diene, and maleimide groups (M), acting as the dienophile, that results in endo and exo stereoisomers of the Diels–Alder cycloadducts (DA).

corresponding rate constants ($k_{DA,endo}$, $k_{rDA,endo}$, $k_{DA,exo}$, and $k_{rDA,exo}$), as schematically shown in Figure 5. These rate constants are functions of temperature and given by the Arrhenius equation (eq 1):

$$k_{DA,i} = A_{DA,i} e^{-E_{DA,i}/RT} \qquad k_{rDA,i} = A_{rDA,i} e^{-E_{rDA,i}/RT} \tag{1}$$

where "i" indicates endo or exo, $A_{DA,i}$ and $A_{rDA,i}$ are the preexponential factors or frequency factors, $E_{DA,i}$ and $E_{rDA,i}$ are the activation energies, R is the universal gas constant, and is T the absolute temperature.

The mathematical representation of the reaction kinetics of this two-equilibrium reaction scheme (Figure 5) consists of a set of ordinary differential equations describing the variation of the concentrations of all components (eqs 2 and 3):

$$\frac{d[M]}{dt} = \frac{d[F]}{dt} = \sum_{i=exo,endo} (k_{rDA,i}[DA_i] - k_{DA,i}[M][F]) = -\frac{d([DA_{exo}] + [DA_{endo}])}{dt} = -\frac{d[DA]}{dt} \tag{2}$$

$$\frac{d[DA_i]}{dt} = k_{DA,i}[M][F] - k_{rDA,i}[DA_i] \tag{3}$$

where $[DA]$ indicates the sum of the concentrations of the exo and endo adducts. These equations can be related to the reaction heat flows ($\dot{q}_r$) through eq 4:

$$\dot{q}_{r,DA_{tot}} = \sum_{i=exo,endo} \{\dot{q}_{r,DA_i}\} = \sum_{i=exo,endo} \left\{ \frac{d[DA_i]}{dt} \Delta_r H_i^0 \right\} \tag{4}$$

in which $\Delta_r H^0_{exo}$ and $\Delta_r H^0_{endo}$ are the standard reaction enthalpies for the formation of the exo and endo DA adducts, respectively. The standard reaction enthalpy $\Delta_r H_i^0$ for the formation of an adduct can be written using the difference in activation energies $E_{rDA,i} - E_{DA,i}$ for that adduct. These equations allow for the derivation of the kinetic parameters of the DA reaction ($A_{DA,i}$, $A_{rDA,i}$, $E_{DA,i}$, and $E_{rDA,i}$) by a nonlinear multiple-parameter least-squares optimization of the simulated heat flows and experimental heat flows measured using DSC (Supporting Information 1). The kinetic parameters used in this work for simulations are listed in Table 1.

The (overall) reaction conversion or extent of the reaction x can be defined by eq 5

Table 1. Kinetic Parameters for the DA Reaction between DPBM and FFJ

kinetic parameter	unit	endo isomer	exo isomer
$\ln A_{DA,i}$	kg·mol^{-1}·s^{-1}	14.3	15.0
$E_{Da,i}$	kJ·mol^{-1}	60.3	65.3
$\ln A_{rDA,i}$	kg·mol^{-1}·s^{-1}	30.2	31.8
$E_{rDA,i}$	kJ·mol^{-1}	108.0	121.0

https://doi.org/10.1021/acs.macromol.2c00434
Macromolecules 2022, 55, 5497–5513

Table 2. Diamine-Based DA Networks with Varying Initial Furan $[F_0]$ (=Maleimide $[M_0]$) Concentration by Changing the Molar Mass M of the Furan-Functionalized Jeffamine (FFJ); the Networks Have a Different DA Concentration at 25 °C ($[DA]_{eq,25°C}$)

monomers	f	M (g·mol^{-1})	M/f (g·mol^{-1})	elastomers	$[M]_0 = [F]_0$ (mol·kg^{-1})	$[DA]_{eq,25°C}$ (mol·kg^{-1})
DPBM	2	358	179			
FD400	4	1081	270	DPBM-FD400	2.19	2.11
FD2000	4	2436	609	DPBM-FD2000	1.25	1.19
FD2000-FD4000-1	4	3316	829	DPBM-FD2000-FD4000-1	0.98	0.93
FD2000-FD4000-2	4	4420	1105	DPBM-FD2000-FD4000-2	0.77	0.73
FD4000	4	5188	1297	DPBM-FD4000	0.67	0.63

$$x = \frac{[DA_{exo}] + [DA_{endo}]}{[M]_0} = \frac{[DA]}{[M]_0} \quad (5)$$

The conversion at equilibrium x_{eq} at a selected temperature can be calculated using the dimensionless concentration-based equilibrium constants ($K_{C,exo}$ and $K_{C,endo}$), which are given in eq 6a

$$K_{C,endo} = \frac{k_{DA,endo}C_0}{k_{rDA,endo}} = \frac{[DA_{endo}]_{eq}C_0}{[F]_{eq}[M]_{eq}}$$

$$K_{C,exo} = \frac{k_{DA,exo}C_0}{k_{rDA,exo}} = \frac{[DA_{exo}]_{eq}C_0}{[F]_{eq}[M]_{eq}} \quad (6a)$$

$$K_{C,DA} = K_{C,endo} + K_{C,exo} = \frac{[DA_{endo}]_{eq}C_0 + [DA_{exo}]_{eq}C_0}{[F]_{eq}[M]_{eq}}$$

$$= \frac{x_{eq}C_0}{\left(\frac{1}{r} - x_{eq}\right)(1 - x_{eq})[M]_0} \quad (6b)$$

in which C_0 is the standard concentration of 1 mol·g^{-1} and $r = [M]_0/[F]_0$ is the maleimide-to-furan molar ratio (also called the stoichiometric ratio). Consequently, the equilibrium conversion x_{eq} can be derived as (eq 7)

$$x_{eq} = \frac{K_{C,DA}\left(1 + \frac{1}{r}\right)[M]_0 + 1 - \sqrt{\left(K_{C,DA}\left(1 + \frac{1}{r}\right)[M]_0 + 1\right)^2 - \frac{4K_{C,DA}{}^2[M]_0{}^2}{r}}}{2K_{C,DA}[M]_0\left(\frac{1}{C_0}\right)} \quad (7)$$

This formula allows us to determine, for every temperature, the equilibrium conversion, which will further, in this paper, be related to mechanical and healing properties.

Diels–Alder Concentration at Room Temperature. The concentration of DA bonds formed at room temperature $[DA]_{eq,25°C}$, increases with the initial concentration of reactive units, maleimide $[M]_0$ and furan $[F]_0$. In this section, only stoichiometric mixtures ($r = [M]_0/[F]_0 = 1$) are considered. The initial concentration $[M]_0$ can be changed by synthesizing reversible networks using furan-functionalized Jeffamines (FFJ) with different molar masses (details in Supporting Information 2). To illustrate the influence of crosslink density on the material properties, five DA networks are synthesized using FFJs with average molar masses ranging from 1081 to 5188 g mol^{-1} (Table 2). All of these FFJs are diamine-based and have four reactive furans per molecule ($f = 4$). Their molar masses are number-average molar masses determined from NMR experiments on the Jeffamines (Supporting Information 3). Intermediate average molar masses can be achieved by mixing two or more FFJs. This is illustrated by mixing the FFJs, FD2000 and FD4000, with molar ratios n_{FD2000}/n_{FD4000} equal to 2.29 and 0.43, to synthesize DPBM-FD2000-FD4000-1 and 2, respectively. For the five synthesized networks, the initial maleimide and furan concentrations and resulting DA adduct concentration at equilibrium at 25 °C, derived using eq 7, are presented in Table 2. The two networks derived by mixing the FFJs illustrate that the crosslink density can be adjusted in a continuous manner.

Changing the maleimide/furan concentration in the network changes the Diels–Alder concentration and therefore the glass-transition temperature T_g of the resulting network, which can be measured by differential scanning calorimetry (DSC) (Figure 6A and Table 3). Upon heating through the glass transition, the cooperative chain segment mobility increases, resulting in a sigmoidal increase in heat capacity, visible as a step in the endothermic direction in the heat flow signal. An increase in concentration, and therefore crosslink density, leads to a decreased flexibility in the network and an increase in T_g (Figure 6B). This increase in T_g with an increase in crosslink density is more pronounced for higher concentrations; as at a low concentration, there is only a limited influence on T_g. This is because at a low crosslink density, the flexibility of the connecting chains is the main controlling parameter, as illustrated by the fitted DiBenedetto model (Figure 6B).

Using dynamic mechanical analysis (DMA), the viscoelastic behavior of the five DA networks was measured over a temperature range of −80 to 100 °C. When increasing the temperature above T_g, all DA networks show a clear drop in both storage modulus, E', and loss modulus, E'', resulting from the increase in cooperative mobility when passing the glass transition (Figure 7A,B). Upon heating above T_g, the storage modulus does not display a rubber plateau of constant or slightly increasing storage modulus, as seen for irreversible polymer networks. Instead, the storage and loss modulus gradually decrease upon heating because the retro-DA reaction is more and more favored and the crosslink density gradually decreases.[38,39] This illustrates the thermoreversibility of the DA crosslinks.

Depending on the position of its T_g in relation to the application temperature (in many cases room temperature T_R), the DA network will exhibit a brittle glassy behavior ($T_g > T_R$) or a flexible elastomer behavior ($T_g < T_R$) at room temperature. DA networks with a high DA concentration will have a T_g higher than the application temperature, as illustrated by DPBM-FD400, which has a T_g at 72 °C and therefore exhibits an almost entirely elastic, glassy behavior at 25 °C. This is further illustrated by a high storage modulus (3.6 GPa), a relatively low loss modulus (164 MPa), and a very low loss angle of only 3°. The DPBM-FD4000 on the other hand has a much lower T_g at −57.8 °C, due to a lower DA concentration (due to a lower initial concentration of furan

https://doi.org/10.1021/acs.macromol.2c00434
Macromolecules 2022, 55, 5497−5513

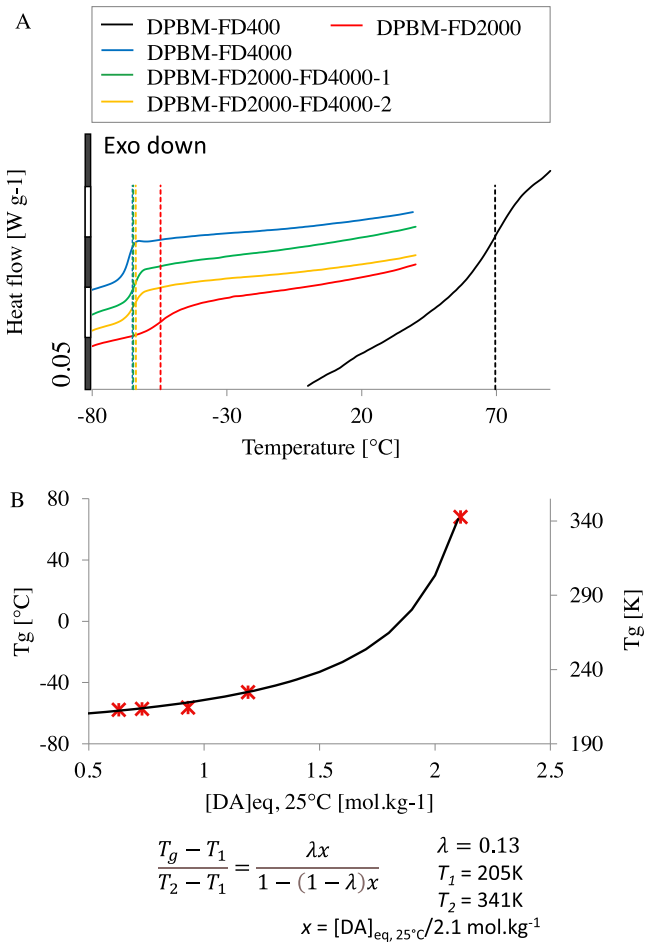

Figure 6. Influence of the DA concentration on the glass-transition temperature (T_g) of DA networks with a stoichiometric ratio of one and FFJs with a furan functionality of four. (A) Differential scanning calorimetry (DSC) measurements at a heating rate of 5 K min^{-1}. Vertical dashed lines represent the T_g's. (B) Experimental (*) and simulated (line) glass-transition temperatures (T_g) of the diamine-based networks as a function of the equilibrium concentration of Diels–Alder bonds at 25 °C, $[DA]_{eq,25°C}$.

and maleimide) and longer flexible chains between them. At 25 °C, DPBM-FD4000 behaves as a flexible rubber with low storage modulus (6.1 MPa), a relatively low loss modulus of (0.76 MPa), and a low loss angle of 7°. This non-negligible loss angle indicates that a viscous component is present in the mechanical response; however, it is limited. This large contrast in mechanical properties illustrates that the DA concentration design parameter allows synthesizing very brittle, stiff self-healing materials down to very flexible, rubbery self-healing materials.

In Figure 7C, for the elastomers, a second transition around 40–50 °C can be observed. This transition most probably originates from physical interactions, possibly to nanoscale phase separation of (reacted) DPBM from the polymer matrix. The networks are made by dissolving the crystalline DPBM and the furan-functionalized Jeffamine in chloroform (details in Supporting Information 4). Once dissolved and mixed, clear and transparent solutions are obtained and films can be made by evaporating the solvent. However, the aromatic bismaleimide is not expected to be very compatible with the aliphatic main chain of the Jeffamines, most likely causing the nanoscale phase separation seen in the DMA results.

In Figure 7D, the storage modulus and loss modulus are plotted as a function of the crosslink density at 25 °C. According to rubber elasticity theory, the elastic modulus increases linearly with crosslink density. Of course, this requires that the T_g is sufficiently below room temperature (e.g., elastomeric networks). However, the storage and loss modulus increase exponentially as a function of DA concentration at 25 °C (Figure 7D). The current exponential relationships show a faster than linear increase with crosslink density in the rubbery state, which can be attributed to a relative increase in the amount of stiffer aromatic DPBM segments with increasing crosslink density. In addition, the results show it is possible to have intermediate properties using combinations of commercially available Jeffamines. If T_g is higher than room temperature, the material is in the vitrified state at 25 °C, and the exponential relationships are no longer applicable.

The influence of the DA concentration on the mechanical properties at 25 °C can also be illustrated by tensile testing up to fracture in strain-controlled experiments (Figure 8A,B). From the resulting engineering stress–strain curve, the Young's modulus E (linear regression in 0–5% strain interval) and the strain and stress at fracture can be derived (Figure 8C,D and Table 3). First, it should be noted that the DA elastomers strain up to 230% prior to fracture (Figure 8A). This makes these materials very interesting for soft robotic applications,[20,26] in which large strains can be reached during actuation.[7] Higher initial maleimide and furan concentrations result in higher crosslinking densities, which increases the fracture stress, as more crosslinks must be broken, while the fracture strain is retained. For the elastomeric networks, the fracture stress-concentration relationship is linear (Figure 8D). In addition, a higher crosslinking density leads to a decrease in flexibility, and an increase in Young's modulus (Figure 8C). For the DA elastomers ($T_g < T_R$), the relation between the Young's modulus and the concentration is again exponential

Table 3. Glass-Transition Temperature (T_g) and Mechanical Properties at 25 °C for the Diamine-Based Networks with Varying DA Concentration at 25 °C[a]

elastomer	$[DA]_{eq,25°C}$ (mol·kg^{-1})	T_g (°C)	E' (MPa)	E'' (MPa)	E (MPa)	σ_{max} (MPa)
DPBM-FD400	2.11	69.5 ± 0.1	3576 ± 120	164 ± 15	1901 ± 56	21.59 ± 0.36
DPBM-FD2000	1.19	−46.3 ± 0.1	104.3 ± 0.7	23.4 ± 0.4	49.3 ± 0.5	5.41 ± 0.07
DPBM-FD2000-FD4000-1	0.93	−56.3 ± 0.1	44.1 ± 0.2	7.30 ± 0.07	22.7 ± 0.2	3.21 ± 0.03
DPBM-FD2000-FD4000-2	0.73	−57.2 ± 0.1	11.50 ± 0.05	2.03 ± 0.02	7.41 ± 0.02	2.06 ± 0.02
DPBM-FD4000	0.63	−57.8 ± 0.1	6.11 ± 0.02	0.76 ± 0.01	4.57 ± 0.03	1.46 ± 0.01

[a]For the Young's modulus (E) and the fracture stress (σ_{max}), standard errors of the mean (SEM) are presented, while for the others, errors based on instrumental accuracy are given.

https://doi.org/10.1021/acs.macromol.2c00434
Macromolecules 2022, 55, 5497–5513

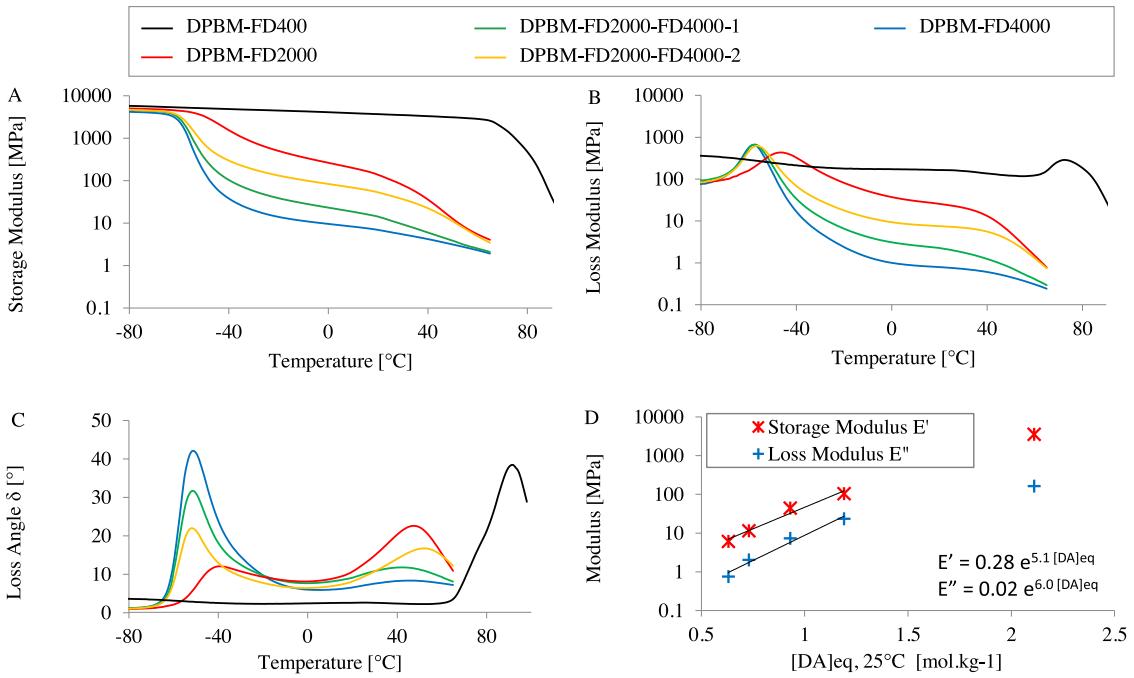

Figure 7. Influence of the DA concentration on the viscoelastic behavior of DA networks. Dynamic mechanical analysis (DMA) measurements performed in heating from −80 to 100 °C at 1 K min^{-1}, using an oscillating strain amplitude of 0.2% and a frequency of 1 Hz, resulting in the (A) storage modulus (E'), (B) loss modulus (E''), and (C) loss angle (δ). (D) Experimentally derived storage modulus (E') and loss modulus (E'') at 25 °C as a function of the equilibrium concentration of DA bonds at 25 °C. The lines are exponential trend lines fitted onto the elastomers' data points.

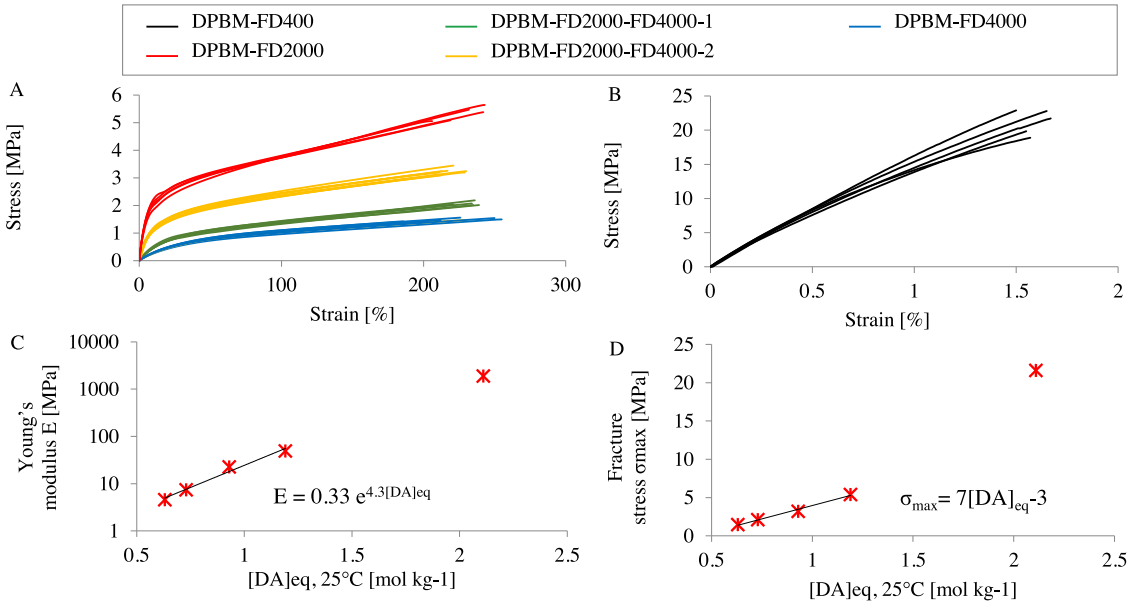

Figure 8. Tensile testing on the five DA networks using a strain ramp of 1 % s^{-1} until fracture. (A, B) Tensile engineering stress as a function of the engineering strain. (C) Young's modulus as a function of the equilibrium DA concentration at 25 °C noted as $[DA]_{eq,25°C}$. The modulus is derived by linear regression in the 0−5% strain window for the elastomers and 0−0.5% strain window for the thermoset. (D) Fracture stress as a function of the equilibrium DA concentration at 25 °C.

(Figure 8C). For the DPBM-FD400 thermoset, having a T_g well above room temperature, the cooperative mobility of the chains is highly restricted, which leads to a much higher Young's modulus of 1.90 GPa and very small strains at fracture of about 1.5% (Figure 8B).

As their mechanical properties can be tuned over a broad range, self-healing DA networks can be applied in both flexible and stiff components. Consequently, the self-healing elastomers were used to manufacture flexible and healable soft bodies for soft robotics,[20] while the thermoset was used to develop a self-healing mechanical fuse.[40] In these applications, large damage, in the centimeter scale, could be healed completely by subjecting the networks to temperatures of 80[20] or 120 °C[40] for 40 min.

In DMA, the viscoelastic behavior was measured as a function of temperature, but this technique is limited to solid

https://doi.org/10.1021/acs.macromol.2c00434
Macromolecules 2022, 55, 5497−5513

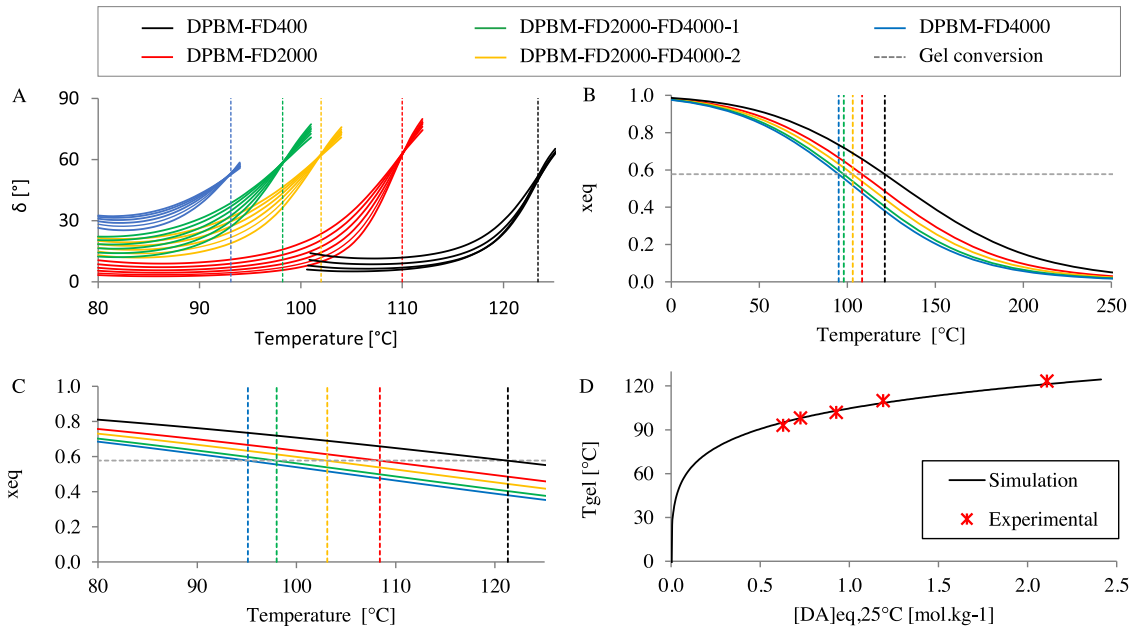

Figure 9. Influence of the initial concentration reactive component on gel conversion x_{gel} and gel-transition temperature T_{gel}. (A) Loss angle δ versus temperature from dynamic rheometry experiments in which the samples were heated at 0.2 K min^{-1} in multifrequency experiments using an oscillating strain with an amplitude of 10% and frequencies of 10, 6.31, 3.98, 2.51, 1.58, and 1 Hz. T_{gel} is the temperature at which the loss angle δ is frequency-independent (intersection isofrequency lines). (B, C) Equilibrium conversion x_{eq} as a function of temperature (eq 7). (D) Experimental (* symbols) and simulated (line) T_{gel} as a function of the equilibrium crosslink density $[DA]_{eq}$ at 25 °C (eq 8).

samples. Upon heating the DA networks above their degelation temperature, the network breaks down into a viscous liquid (Figure 3). Hence, dynamic rheometry was used to expand the temperature region (Supporting Information 5). As in dynamic rheometry, the degelation temperature, T_{gel}, is best defined as the temperature at which δ is frequency-independent,[29] the materials were subjected to a multifrequency dynamic rheometry experiment. An oscillating strain with an amplitude of 10% and frequencies of 10, 6.31, 3.98, 2.51, 1.58, and 1 Hz were applied, while the temperature was increased from 80 to 130 °C with a temperature ramp of 0.2 K min^{-1}. At these slow heating rates, the material is at each temperature under near-equilibrium condition, as proven in Supporting Information 5. The resulting loss angle (δ) is plotted as a function of temperature in Figure 9A, while the resulting storage moduli and loss moduli are presented in Figure S12. T_{gel} can be identified as the temperature at which the isofrequency lines cross over, which corresponds with δ being frequency-independent.

According to Flory−Stockmayer,[41,42] the critical gel conversion is defined by eq 8

$$x_{gel} = \frac{1}{\sqrt{r(f_M - 1)(f_F - 1)}} \quad (8)$$

For the diamine-based networks (Table 2), having a maleimide functionality f_M of 2, a furan functionality f_F of 4, and a stoichiometric maleimide-to-furan ratio r of 1, this gel conversion x_{gel} is 0.577. At conversions lower than x_{gel}, no network structure is present and the polymer exhibits viscous liquid behavior. In Figure 9B, for each of the five networks, the equilibrium conversion, calculated using eq 7, is plotted as a function of temperature. The simulated equilibrium T_{gel} is defined as the temperature at which the equilibrium conversion is equal to the gel conversion as defined by eq 8. To validate this simulated equilibrium T_{gel}, relying on the kinetics of Table 1, Figure 9C compares the simulated T_{gel} for networks with $[DA]_{eq,25°C}$ ranging from 0 to 2.5 mol kg^{-1} with the experimental T_{gel} obtained by dynamic rheometry. Higher crosslink densities shift the equilibrium conversion curve to higher temperatures (Figure 9B) and lead to an increase in T_{gel} (Figure 9C). As the simulated and experimentally derived T_{gel} correspond very well, the combination of the equilibrium conversion, calculated using the eq 7 and the kinetic parameters (Table 1), with the Flory−Stockmayer equation (eq 8), allows for simulating the Diels−Alder reaction and the gel transition quite accurately. Using the kinetics parameters, time-based simulations that rely on solving the coupled rate equations (eqs 2 and 3), can be used to estimate (de)gelation based on temperature−time profiles. Such simulations are an excellent tool to derive processing settings for manufacturing techniques for Diels−Alder networks, as illustrated by the optimization of temperature profiles for extrusion and fused filament fabrication 3D printing.[35]

Healing is facilitated by reactivity as well as mobility. The latter is required to create good contact on the microscopic level. Although healing below T_g in DA thermosets has been proven,[43] healing in the order of hours can only be achieved by heating well above T_g, resulting in an increase in mobility. The thermoset DPBM-FD400 heals in 40 min at 119.5 °C with efficiencies of 90−100%.[40] The DPBM-FD2000 and FD4000 can heal at much lower temperatures, due to an increased portion of reactive maleimide and furan, seen as a lower x_{eq} as a function of temperature (Figure 9B) and a higher mobility, expressed in lower mechanical moduli (Table 3). As a result, DPBM-FD4000 heals already at 80 °C for the same 40 min, reaching high efficiencies of 98−99%.[20] Consequently, mobility plays a crucial role during healing, and therefore higher crosslinked networks, with a higher DA concentration, heal at higher temperatures for a given healing time.

https://doi.org/10.1021/acs.macromol.2c00434
Macromolecules 2022, 55, 5497−5513

Table 4. DA Networks with a Different Functionality of the Furan-Functionalized Jeffamine

monomers	f	M (g·mol^{-1})	M/f (g·eq^{-1})	elastomers	$[M]_0 = [F]_0$ (mol·kg^{-1})	$[DA]_{eq,25°C}$ (mol·kg^{-1})
DPBM	2	358	179			
FT5000	6	7626	271	DPBM-FT500	0.77	0.72
FD2000-FD4000-2	4	5080	1270	DPBM-FD2000-FD4000-2	0.77	0.72

Functionality. Changing the functionality of the monomer units influences the gel conversion (eq 8), but also affects the viscoelastic properties of the resulting networks at higher temperatures. This will be illustrated by comparing two networks, DPBM-FT5000 and DPBM-FD2000-FD4000-2, differing in the functionality of the furan compound, while having the same maleimide-to-furan ratio of 1 and the same DA concentration at room temperature. (Table 4). Consequently, at room temperature, they have very similar mechanical properties, as illustrated by nearly identical tensile curves (Figure 10), fracture stress, and Young's modulus (Table 5).

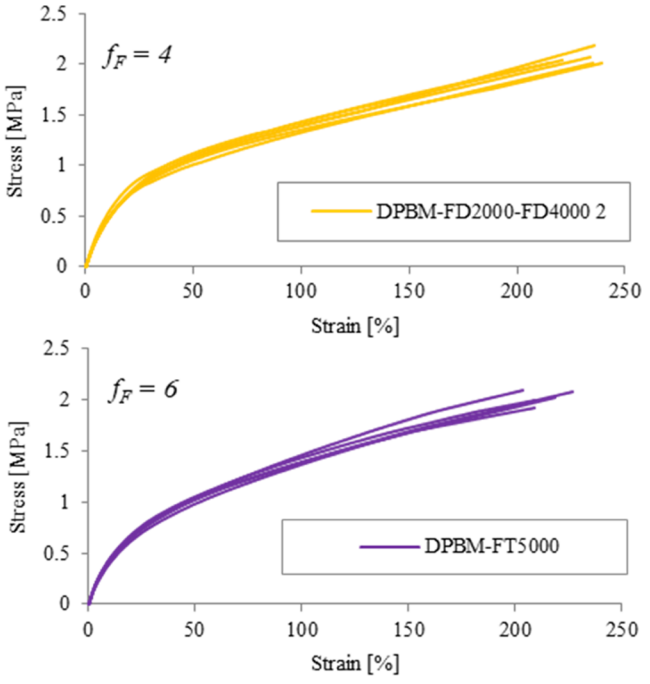

Figure 10. Influence of the furan functionality (f_F) on the mechanical behavior of DA networks: tensile tests on DPBM-FD2000-FD4000-2 (yellow) and DPBM-FT5000 (purple), using a strain ramp of 1% s^{-1} until fracture. The resulting engineering stress is plotted as a function of the engineering strain.

Over the temperature range of −80 to 65 °C, the elastomeric networks have a very similar viscoelastic behavior, as confirmed by DMA (Figure 11A−C). T_g, Young's modulus (E) measured in tensile testing, and the storage modulus (E'), loss modulus (E''), and loss angle (δ) at 25 °C measured in DMA are comparable (Table 5). The slightly lower flexibility of the triamine-based network, DPBM-FT5000, is attributed to the extra irreversible crosslink per FFJ molecule introduced by the branching point in the triamine. DMA and DSC measurements illustrate that the glass-transition temperatures are within a 1 K difference (Figure 11D and Table 4). Clearly, these two elastomers can be used for the same applications at room temperature and below.

With increasing temperature and decreasing DA adduct concentration, the contribution of the irreversible crosslinks in the network to the mechanical properties increases. Consequentially, the DPBM-FT5000 network is more mechanically stable at higher temperatures. This increase in mechanical stability at higher temperatures due to a higher functionality is confirmed by dynamic rheometry on both networks (Figure 12A). The most important effect of the functionality is on the gel-transition temperature T_{gel}: the triamine-based DPBM-FT5000 network degels at 118 °C, which is 20 °C higher than the T_{gel} of 98 °C of the diamine-based DPBM-FD2000-FD4000-2 network (Figure 12A). The functionality does not affect the reaction kinetics and therefore does not influence the DA conversion (Figure 12A,B). A higher functionality f results in a lower gel conversion x_{gel}, as seen in the Flory−Stockmayer eq 8 and illustrated in Figure 12D, and consequently, in a higher gel-transition temperature T_{gel} (Figure 12B). The T_{gel} measured in rheometry corresponds nicely with the T_{gel} calculated as a function of the furan functionality f_F for networks with an initial maleimide and furan concentration of 0.77 mol kg^{-1} (Figure 12D), calculated using eqs 6a−8 and the kinetic parameters of Table 1.

The results of Figures 10−12 clearly indicate that the functionality f parameter allows for tuning the gelation conversion and temperature, while having a limited effect on the mechanical properties at room temperature and below. Consequently, this parameter can be used to design the DA polymers to fit a specific manufacturing technique. For example, for fused filament fabrication (FFF), a 3D printing technique, a high T_{gel} is preferred.[35] During printing, the DA polymer is heated a few degrees above T_{gel} in the printing head and nozzle and is deposited on a print bed on which it should quickly gel and reform the network. Materials having a higher T_{gel}, can be printed at higher temperatures, where the kinetics of the DA reaction are faster. As a result, the polymer solidifies faster during printing and print speeds can be increased. The fact that the gel-transition temperature can be controlled

Table 5. Glass-Transition Temperature (T_G) and Mechanical Properties at 25 °C from DMA (E', E'', and δ) and Tensile Testing (E and σ_{max}) for Networks Based on FFJs with a Different Furan Functionality[a]

elastomer	T_g (°C)	E' (MPa)	E'' (MPa)	δ (deg)	E (MPa)	σ_{max} (MPa)
DPBM-FT5000	−64.3 ± 0.1	16.74 ± 0.05	2.43 ± 0.01	8.26 ± 0.03	8.20 ± 0.09	1.97 ± 0.02
DPBM- FD2000-FD4000-2	−63.8 ± 0.1	11.50 ± 0.06	2.00 ± 0.01	10.01 ± 0.04	7.41 ± 0.02	2.05 ± 0.02

[a]For the Young's modulus (E) and fracture stress (σ_{max}), standard errors of the mean (SEM) are presented, while for the others, errors based on instrumental accuracy are given.

https://doi.org/10.1021/acs.macromol.2c00434
Macromolecules 2022, 55, 5497−5513

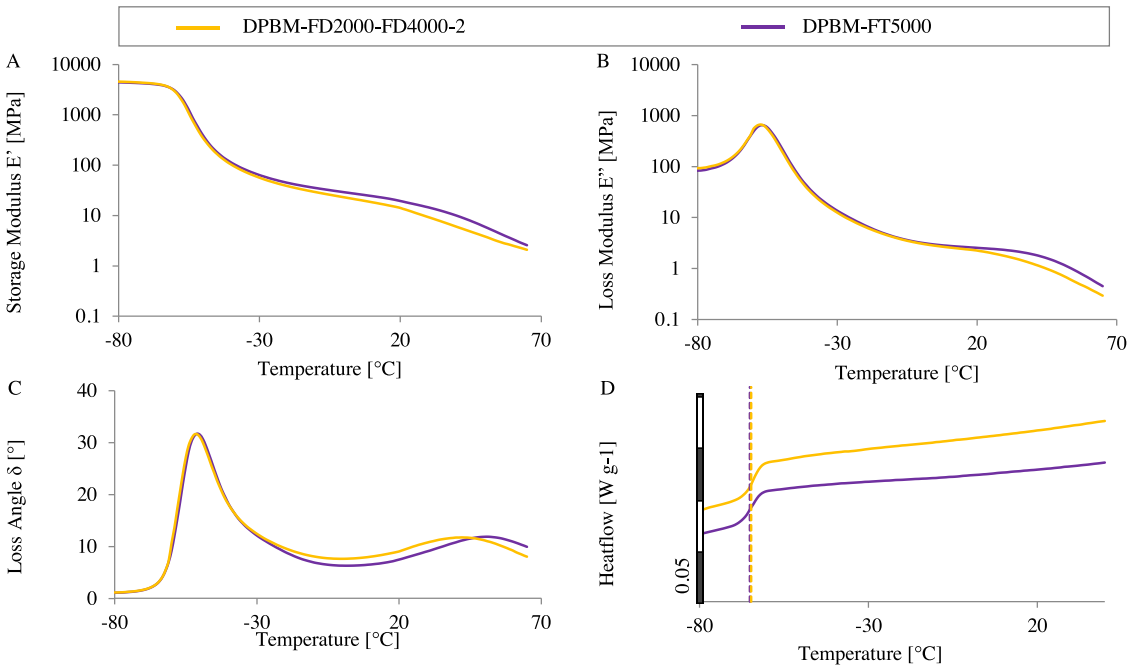

Figure 11. Influence of the furan functionality on the viscoelastic behavior of DA networks. Storage modulus E' (A), loss modulus E'' (B), and loss angle δ (C) from DMA measurements in heating from −80 to 100 °C at 1 K min^{-1}, using an oscillating strain with 0.2% amplitude and a frequency of 1 Hz. (D) DSC pattern at a heating rate of 5 K min^{-1}.

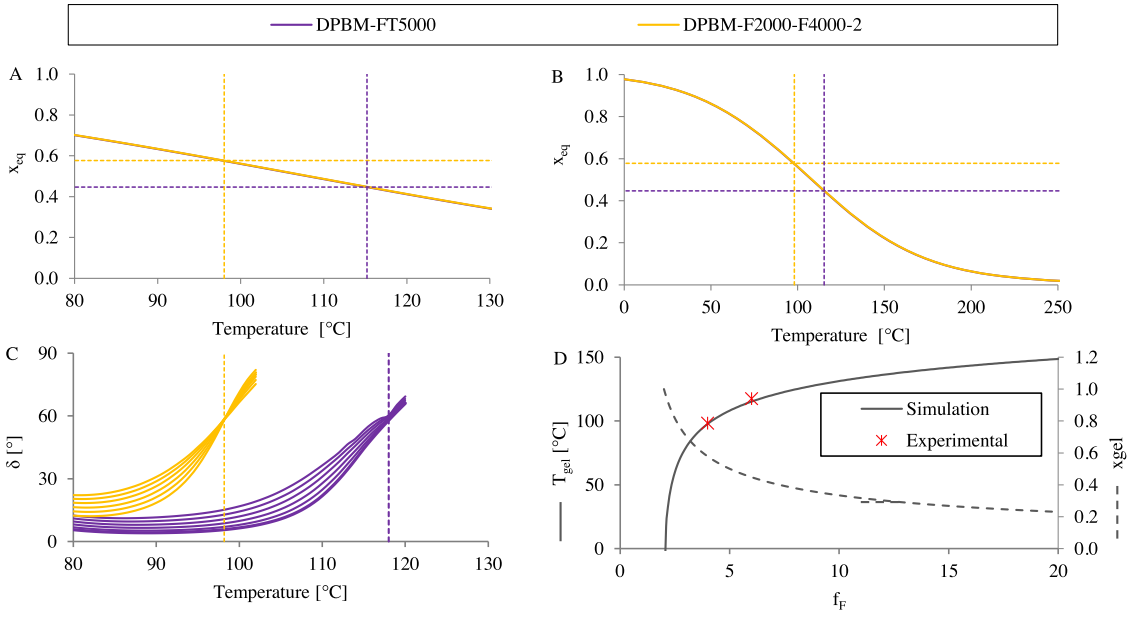

Figure 12. Influence of the furan functionality f_F on the gel conversion x_{gel} and gel-transition temperature T_{gel}. (A, zoom of B) Equilibrium conversion x_{eq} as a function of temperature calculated using eq 7. The simulated equilibrium T_{gel} is defined as the temperature at which x_{eq} is equal to the gel conversion (eq 8). (C) Loss angle δ versus temperature from dynamic rheometry and experimental T_{gel} (dotted lines). (D) Simulated equilibrium gel conversion x_{gel} and experimental T_{gel} (* symbols) and simulated T_{gel} (line) as a function of furan functionality f_F of the FFJ for networks with the same initial maleimide and furan concentration of 0.77 mol kg^{-1}.

independently from the mechanical properties at application temperature provides an interesting degree of freedom for designing networks that suit both manufacturing techniques and application requirements. In this paper, the furan functionality f_F of the FFJ was varied; however, changing the functionality of maleimide-containing monomer f_M will affect the material properties in a similar way.

As healing is dictated by both mobility and reactivity, networks that only differ in functionality have a very similar healing behavior. This results from the identical number of reactive maleimide and furan in the network for a given temperature (Figure 12B) and mobility, represented by the mechanical properties as a function of temperature (Figure 11).

Stoichiometry. To illustrate the effect of the third network design parameter, the molar ratio between the initial maleimide and furan reactive groups r (eq 6a), two networks, DPBM-FT5000-r0.83 and DPBM-FT3000-r0.52, with equal

https://doi.org/10.1021/acs.macromol.2c00434
Macromolecules 2022, 55, 5497−5513

Table 6. DA Networks with Different Maleimide-to-Furan Molar Ratios *r*

monomer	f	M/f (g·mol^{-1})	elastomer	r	$[M]_0$ (mol·kg^{-1})	$[F]_0$ (mol·kg^{-1})	$[DA]_{eq,25°C}$ (mol·kg^{-1})	$[M]_{eq,25°C}$ (mol·kg^{-1})	$[F]_{eq,25°C}$ (mol·kg^{-1})
DPBM	2	179							
FT5000	6	1114	DPBM-FT5000	0.83	0.65	0.79	0.64	0.01	0.14
FT3000	6	689	DPBM-FT3000	0.52	0.64	1.25	0.64	0.00	0.61

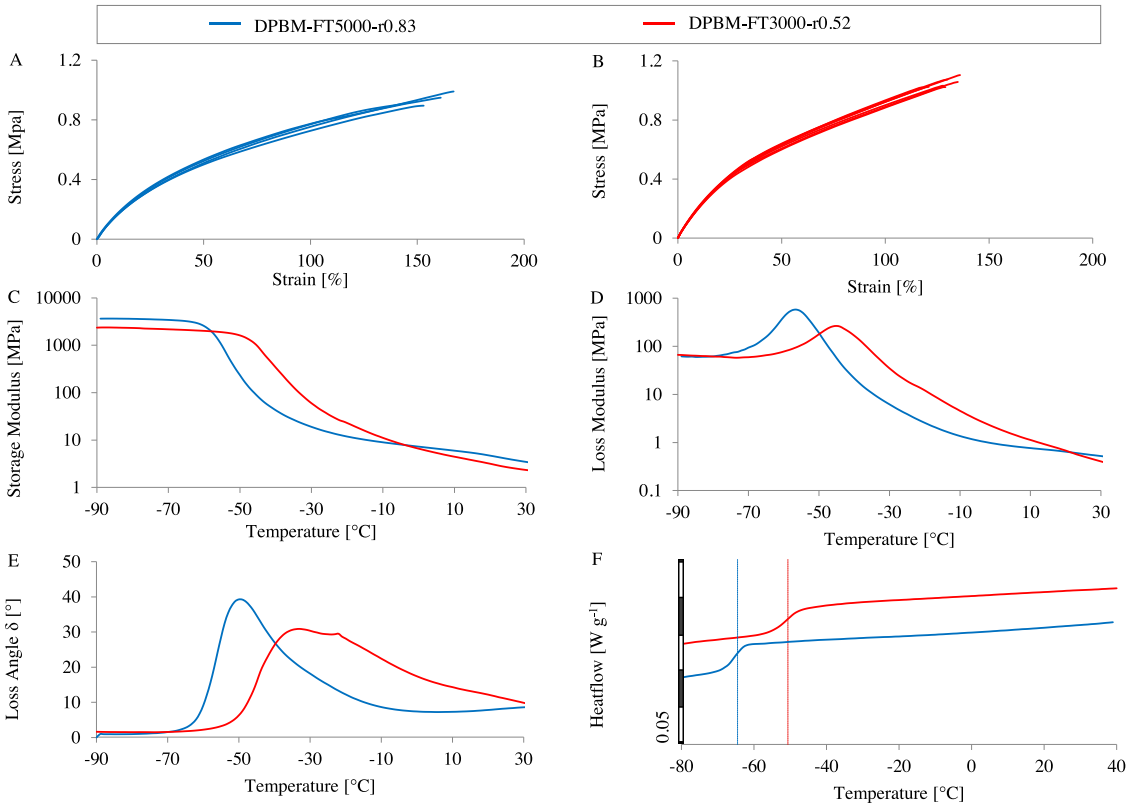

Figure 13. Effect of the molar maleimide-to-furan molar ratio r on the mechanical properties of the DA network, illustrated by DPBM-FT5000-*r*0.83 and DPBM-FT3000-*r*0.52. (A, B) Tensile testing using a strain ramp of 1 % s^{-1} until fracture. The resulting engineering stress is plotted as a function of engineering strain. Storage modulus E' (C), loss modulus E'' (D), and loss angle δ (E) from DMA measurements performed in heating from −90 to 100 °C at 1 K min^{-1}, using an oscillating strain with 0.2% amplitude and a frequency of 1 Hz. (F) DSC pattern at a heating rate of 5 K min^{-1}.

Table 7. Glass-Transition Temperature (T_g) and Mechanical Properties at 25 °C for Networks with Varying Stoichiometric Maleimide-to-Furan Ratio *r*[a]

elastomer	T_g (°C)	E' (MPa)	E'' (MPa)	δ (deg)	E (MPa)	σ_{max} (MPa)
DPBM-FT5000-*r*0.83	−64.1 ± 0.1	3.98 ± 0.05	0.58 ± 0.01	8.35 ± 0.03	2.08 ± 0.01	0.94 ± 0.02
DPBM-FT3000-*r*0.52	−50.4 ± 0.1	3.14 ± 0.07	0.58 ± 0.02	10.26 ± 0.04	2.36 ± 0.02	1.03 ± 0.01

[a]For the Young's modulus (E) and fracture stress (σ_{max}), standard errors of the mean (SEM) are presented, while for the others, errors based on instrumental accuracy are given.

DA crosslink density at 25 °C, $[DA]_{eq,25°C}$, equal maleimide and furan functionalities, but a different maleimide-to-furan ratio r, are compared (Table 6). To achieve the same $[DA]_{eq,25°C}$, r values were selected for the FT5000- and FT3000-based networks using eq 7. As FT3000 has a lower molar mass per functionality, this leads to DPBM-FT3000-*r*0.52 having a larger excess of furan groups remaining $[F]_{eq}$ in its network. In other works, the stoichiometric ratio r is altered by changing the ratio between the monomers used.[27,28] However, in that case also, the DA concentration at 25 °C is affected. To the best of our knowledge, this paper is the first to show the effect of stoichiometry on the material properties, while keeping the DA concentration at 25 °C and monomer functionalities constant.

At 25 °C, the networks have the same crosslink density, which leads to similar stress−strain curves in tensile testing (Figure 13A,B) and comparable Young's moduli and fracture stresses (Table 7). In addition, at room temperature, they have similar storage modulus (E'), loss modulus (E''), and loss angle (δ), as observed using DMA (Figure 13C−E). Consequently, based on their mechanical properties (Table 7), these networks can be used for the same application at room temperature.

When decreasing the temperature below room temperature, the crosslink densities in the network remain identical for the two networks (conversions $x_{eq} \approx 1$). Yet, upon cooling below

https://doi.org/10.1021/acs.macromol.2c00434
Macromolecules 2022, 55, 5497−5513

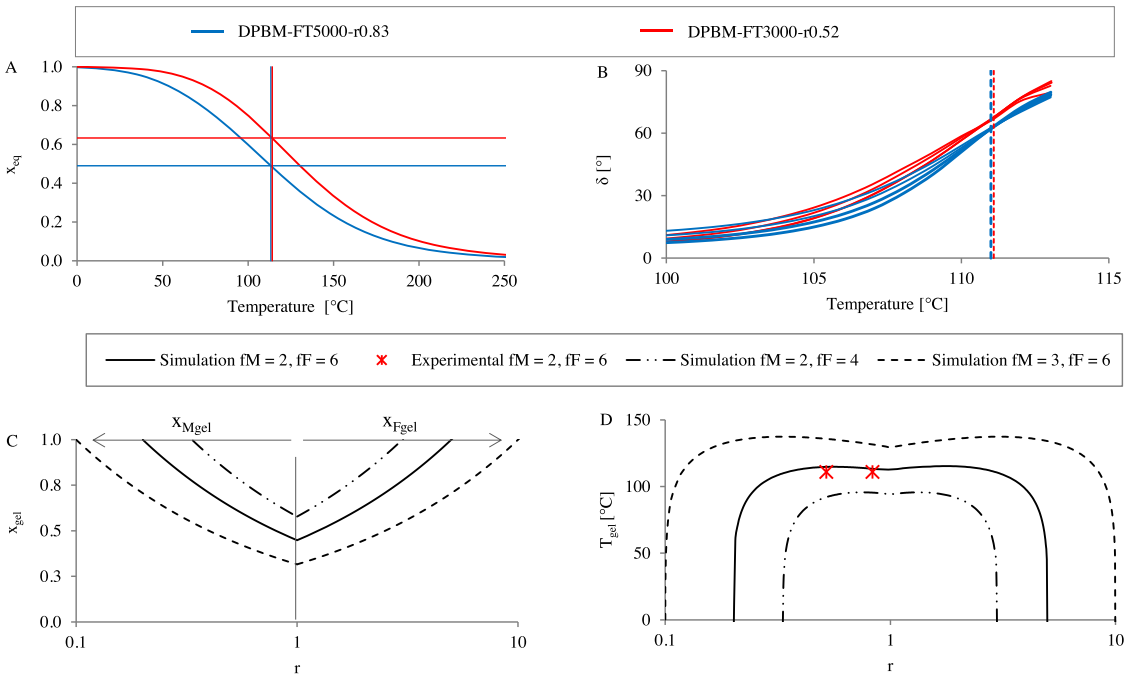

Figure 14. Effect of the maleimide-to-furan molar ratio r on the equilibrium conversion x_{eq}, gel conversion x_{gel}, and gel-transition temperature T_{gel} for elastomers with a $[DA]_{eq,25}$ of 0.64 mol kg^{-1}. (A) Equilibrium conversion x_{eq} as a function of temperature calculated using eq 7. (B) Loss angle δ versus temperature from dynamic rheometry experiments in which the samples were heated at 0.2 K min^{-1} in multifrequency experiments using an oscillating strain with an amplitude of 10 % and frequencies of 10, 6.31, 3.98, 2.51, 1.58, and 1 Hz. T_{gel} is the temperature at which the loss angle δ is frequency-independent (intersection isofrequency lines). Simulated x_{gel} (C) and T_{gel} (D) as a function of molar ratio r for networks with different maleimide (f_M) and furan (f_F) functionalities. The simulated equilibrium T_{gel} is defined as the temperature at which x_{eq} is equal to the gel conversion defined by the Flory–Stockmayer equation (eq 8). The experimental T_{gel} values are indicated by symbols (*).

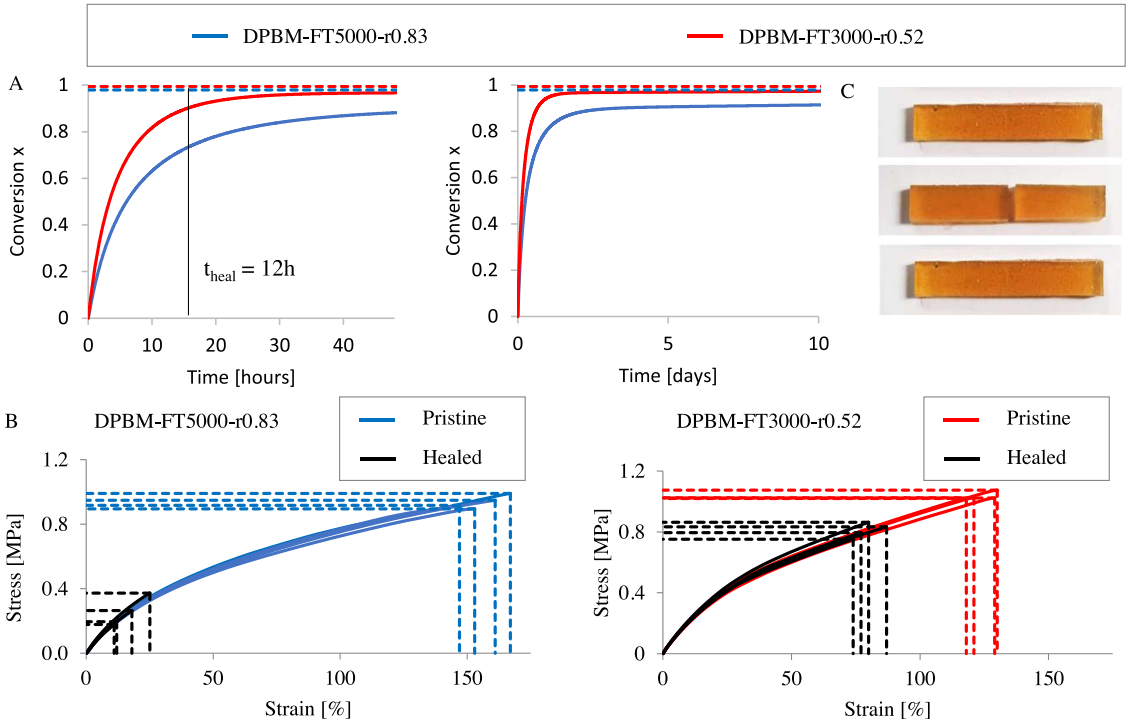

Figure 15. Effect of the stoichiometric ratio r on the reaction speed and healing speed. (A) Simulation of the increase in conversion x as a function of time at 25 °C, in the DPBM-FT5000-r0.83 and DPBM-FT3000-r0.52 networks, starting from zero conversion. (B) Tensile testing until fracture with a strain ramp of 1 % s^{-1} on undamaged pristine samples as well as on samples that underwent a damage–heal cycle. (C) To damage the samples, they were cut in half using a scalpel blade. The fracture surfaces were brought immediately back in contact and the samples were healed for 12 h at 25 °C. Pictures are of the DPBM-FT3000-r0.52 material.

https://doi.org/10.1021/acs.macromol.2c00434
Macromolecules 2022, 55, 5497–5513

Table 8. Healing Efficiencies Based on the Recovery of Mechanical Properties after Healing[a]

elastomer	$[DA]_{t=12h}$ (mol·kg^{-1})	$x_{t=12h}$	$\eta(E)$ (%)	$\eta(\sigma_f)$ (%)	$\eta(\varepsilon_f)$ (%)
DPBM-FT5000-*r*0.83	0.442	0.675	102 ± 3	27 ± 3	11 ± 1
DPBM-FT3000-*r*0.52	0.552	0.856	102 ± 2	78 ± 2	64 ± 2

[a]Samples were cut in half and healed for 12 h at 25 °C. Crosslink densities and conversions were simulated based on the isothermal of 12 h. Standard errors of the mean (SEM) are presented.

25 °C, the storage modulus (E') and loss modulus (E'') increase much faster for the lower *r*-value network, the DPBM-FT3000-*r*0.52 (Figure 13C,D). This is explained by the higher rigidity of the chain ends of the FFJs compared to the mid-chain segments, illustrated by the higher glass transition of FFJs with lower molar weight (Supporting Information 4, Figure S10). As a result, a higher number of chain ends (unbound furan) in the network leads to less mobility. This is translated into a higher glass-transition temperature T_g both seen in DMA (Figure 13D, maximum in the loss modulus) and DSC (Figure 13F and Table 7).

As the excess of furan groups pushes the thermodynamics toward the formation of the DA bonds (eq 7), the equilibrium conversion x_{eq} curve at temperatures above 25 °C will be higher for lower molar ratios *r* (Figure 14A), resulting in a slower decrease of the crosslink density $[DA]_{eq}$ and thus more thermally stable properties. The gel-transition temperature T_{gel} (Figure 14C), at which the equilibrium conversion x_{eq} equals the gel conversion x_{gel}, depends on the maleimide-to-furan molar ratio *r*, in addition to the functionalities f_M and f_F, as stated in the Flory−Stockmayer equation (eq 8). Lower molar ratios *r* result in higher x_{gel}. As x_{eq} and x_{gel} both change to higher values, T_{gel} is almost identical for these networks (Figure 14A), as confirmed experimentally by dynamic rheometry measurements (Figure 14B).

In Figure 14D, T_{gel} is simulated as a function of the maleimide-to-furan ratio *r* for networks with a crosslink density at 25 °C of 0.64 mol kg^{-1} and for different maleimide (f_M) and furan (f_F) functionalities. Looking at the networks with f_M of 2 and f_F of 6, T_{gel} is influenced by *r*, but mainly at values below 0.25 and above 2. Between these values, the influence on T_{gel} is more limited, as is confirmed by the limited experimental difference observed for DPBM-FT5000-*r*0.83 and DPBM-FT3000r-*r*0.52 (Figure 14A,B). The curve goes through a maximum T_{gel} for both $r < 1$ and $r > 1$, as a result of both x_{gel} and x_{eq} shifting with varying magnitudes as a response to the changing *r*. Changing the functionality of monomers in this region, however, results in a much larger change in T_{gel}, as is illustrated in Figure 14D.

The maleimide-to-furan ratio *r* also affects the reaction kinetics of the DA reaction. In previous work, it was reported how a decreasing molar ratio of the starting monomers (e.g., decreasing both *r* and $[DA]_{eq,25°C}$) leads to a decrease in both the equilibrium conversion and the rate at which it was attained during synthesis and healing.[28] In this work, special attention was given to keeping the DA concentration at 25 °C constant to study the effect of the stoichiometric ratio alone on the reaction kinetics. This is illustrated by simulating the formation of DA networks DPBM-FT5000-*r*0.83 and DPBM-FT3000-*r*0.52: Figure 15A shows the increase in conversion $x = [DA]/[M_0]$ at 25 °C, starting from an initial state with conversion equal to zero. The higher excess of furan in the DPBM-FT3000-*r*0.52 network leads to a much faster increase of conversion towards the equilibrium conversion at 25 °C (dotted line in Figure 15A). The higher furan concentration [F], resulting from the excess of furan reactive groups, leads to faster DA reactions (eqs 2 and 3) at the start of the process, and an even stronger increase in the reaction rate at high conversions, as can be seen by comparing the slopes of these curves at, e.g., 85% of conversion. This strong effect in the final stages results from the fact that the concentration of the excess component does not decrease as much, relatively speaking: at 85% conversion, the maleimide concentration decreased to 15% of its original value, while the furan concentration reduced to 29 and 56% of its original value, for molar ratios of 0.83 and 0.52, respectively. This is leading to the DA reactions being 2.0 and 3.7 times faster, for molar ratios of 0.83 and 0.52, respectively, compared to a stoichiometric elastomers with molar ratio 1.

This increased reactivity as a result of the excess in furan reactive groups further speeds up the network formation after mechanical damage to the network structure, resulting in faster healing. Under the hypothesis that all reversible bonds are broken at the fracture surface, the local conversion is zero after damage. When bringing fracture surfaces immediately back in contact at 25 °C, the formation of bonds across the fracture interface will be much faster in networks with an excess of furan reactive groups, as simulated in Figure 15A. This is confirmed experimentally by tensile testing on pristine and healed samples (Figure 15B). For both networks, four pristine samples were fractured in a tensile test with a strain ramp of 1% s^{-1}. Four other samples were cut in half with a scalpel blade, after which they were brought in contact immediately (Figure 15C). These samples were left to heal for 12 h at 25 °C and subsequently tested to fracture in the tensile tester. As is clear from Figure 15B and Table 8, the recovery of the mechanical properties after healing is much better for DPBM-FT3000-*r*0.52. While for the DPBM-FT5000-*r*0.83 the stress at fracture has recovered to 27% of its initial value, for the DPBM-FT3000-*r*0.52, this property has recovered to 78% of its initial value. This is attributed to the (difference in) conversion reached after 12 h of healing at 25 °C, which is 0.67 and 0.86 for DPBM-FT5000-*r*0.83 and DPBM-FT3000-*r*0.52, respectively.

This illustrates well how the healing performance of a DA network can be increased by an excess of furan end-groups. As shown in a previous research article,[33] longer healing times at 25 °C eventually lead to almost complete recovery of the initial properties, with healing efficiencies of 91 and 97% for the stress at fracture of damaged DPBM-FT5000-*r*0.5 samples healed for 7 and 14 days, respectively. The DPBM-FT5000-*r*0.5 has a higher chain segmental mobility and larger excess of furan groups than the DPBM-FT5000-*r*0.83, allowing for successful recovery of the mechanical properties under ambient conditions. Similarly, the healing performance could be increased by an excess of maleimide ($r > 1$), as this would also lead to a slower relative decrease of the excess concentration (eqs 2 and 3). However, to do this maleimides with higher functionality ($f_M > 2$) are needed.

https://doi.org/10.1021/acs.macromol.2c00434
Macromolecules 2022, 55, 5497−5513

Despite the general misconception that reversible covalent polymer networks, such as those based on the DA chemistry, are non-autonomous self-healing materials,[44] the experiments clearly show that this excess of reactive compounds allows us to create DA networks that heal at room temperature. This is interesting for soft robotic applications as this avoids the need of an additional heating system, thus decreasing the complexity of the system. A soft robotic hand was constructed out of a DA network DPBM-FT5000-*r*0.5, that completely recovers its performance after damage in the centimeter scale within minutes to days at room temperature, depending on the magnitude and location of the damage.[33]

Networks with a higher r value, for example, with stoichiometric compositions (r = 1), can heal as well, but increasing the temperature is required to speed up the kinetics of the DA reaction to perform healing in a reasonable amount of time, e.g., in the order of hours, and to achieve the desired healing efficiency. This is illustrated by healing tests on the DPBM-FT5000-*r*1 and DPBM-FT5000-*r*0.83 networks presented in Figure 16. Samples were cut in half and were heated

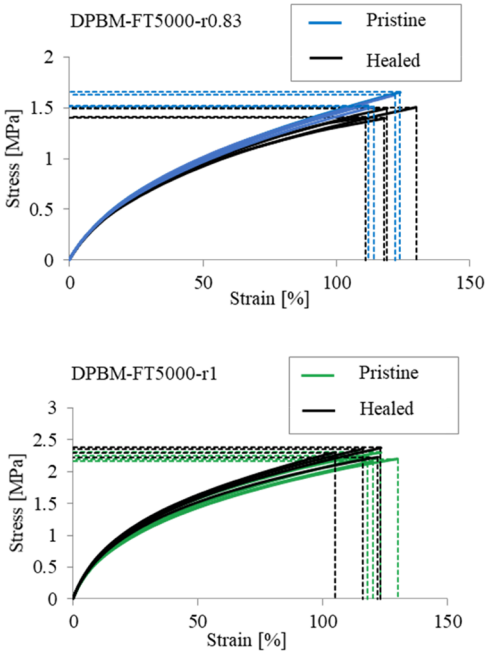

Figure 16. Healing tests on non-autonomous self-healing DA networks, DPBM-FT5000-*r*0.83 and *r*1, through tensile tests until fracture with a strain ramp of 1% s^{-1} on pristine samples and on samples that underwent a damage−heal cycle, including 40 min at 80 °C (healed).

to 80 °C for 40 min and left at room temperature for 16 h, after which they healed with high healing efficiencies close to 100% (Table 9). An advantage of stimulus-induced healing for soft robotics[20,26] is a higher degree of control over the healing procedure[7] and healing can be performed at a suitable instant. For autonomous healing, the healing is preferred to occur immediately.[33]

Table 9. Healing Efficiencies Based on the Recovery of Mechanical Properties after Healing[a]

elastomer	$\eta(E)$ (%)	$\eta(\sigma_f)$ (%)	$\eta(\varepsilon_f)$ (%)
DPBM-FT5000-*r*0.83	97 ± 1	92 ± 2	101 ± 3
DPBM- FT5000-*r*1.00	105 ± 2	104 ± 1	95 ± 3

[a]Samples were cut in half and healed at 80 °C for 40 min. Standard errors of the mean (SEM) are presented.

DISCUSSION

It was illustrated that by changing the network design parameters, the material properties of the resulting Diels−Alder-based (DA) networks can be tuned over a broad range. By changing the *DA crosslink density* (expressed as the concentration of DA adducts [DA]), while keeping the other network design parameters constant, the mechanical properties at room temperature, which is in most cases the application temperature, can be tuned over several orders of magnitudes, with the Young's modulus ranging from MPa to GPa. Consequently, these networks can be used in diverse applications, as highly crosslinked DA networks lead to stiff, yet healable components that can be used in robotics applications,[40] while less crosslinked DA networks have an elastomeric behavior, which allows them to be used to manufacture healable soft robots.[20] By combining FFJs with different molar masses, the crosslink density can be changed in a continuous manner between the limits of the networks obtained using the shortest and the longest furan-functionalized monomers. This broad range and the knowledge of the effect of this DA concentration on the mechanical properties permits fine-tuning the DA networks to fit requirements imposed by applications, such as healable robotic components.[7] The healing temperature is influenced by the DA concentration as well. Higher concentration leads to a decrease in mobility, pushing the healing temperature to higher temperatures.

By changing the *functionality* of the monomers, while keeping the other parameters constant, the reversible gel-transition temperature can be altered while the mechanical properties at room temperature remain the same. A higher functionality pushes (de)gelation to higher temperatures. For elastomers, the functionality has only a limited effect on the mechanical properties, and consequently, this network design parameter allows us to partially decouple the fine-tuning of the mechanical properties at the application temperature from adapting the gel-transition temperature that determines the manufacturing temperature. For manufacturing through molding, low degelation temperatures can be favorable, as less heat is required to make the material flow, which can have economic and ecological benefits. In contrast, in fused filament fabrication, high degelation temperatures are preferred, as at higher printing temperatures, the speed of solidification can be increased, favoring higher print speeds.[35]

By modifying the *stoichiometric ratio* between the maleimide and furan groups, while keeping the other parameters constant, mainly the reaction speed and healing rate are affected. A lower maleimide-to-furan molar ratio results in an excess of furan reactive groups and leads to faster DA bond formation, and hence, faster healing. It is illustrated that the stoichiometric ratio can be used to speed up the healing process while keeping the mechanical properties at application temperatures and the gel-transition temperatures hardly unchanged. It was proven that for DA networks with a high excess of furan, healing can be achieved at room temperature within hours. Such autonomous intrinsic healing is desired in many applications, as it eliminates the need for an external heat stimulus and a system to provide it, as demonstrated previously for a soft robotic hand.[33] Non-autonomous healing, meanwhile, provides

https://doi.org/10.1021/acs.macromol.2c00434
Macromolecules 2022, 55, 5497−5513

opportunities for excellent control over the timing of the healing procedure. This is desired in (robotics) applications in which partially damaged components can continue operation with reduced performance or a compensated behavior[45] and healing can be scheduled when less or no activity is required.[7] The stoichiometric ratio network design parameter will allow us to tune the healing time and temperature of DA networks to match the requirements imposed by the application.

In addition to the three network design parameters defined in this paper, the flexibility of the polymer segments in the network can be altered using monomers with another backbone in the synthesis, influencing the mechanical and (chemo)rheological properties. Although not addressed in this work, changing the reversible chemistry used for the crosslinking will impact the mechanical strength as well as the reactivity and therefore the healing rate, as illustrated by the difference in kinetics parameters between the DPBM-FFJ system (Table 1) and a system composed of poly(propylene oxide) 400 bismaleimide (M400) and FFJ.[32]

Aside from healing and recyclability, addressed in previous work,[20] the reversible DA crosslinks present in the DA networks provide the additional advantage of excellent interfacial bonding: DA networks with different mechanical properties can be joined by a heat−cool cycle. The result is a multimaterial component with strong interfacial bonding due to the formation of covalent DA bonds across material boundaries. In many applications, the repeated occurrence of stress concentrations at interfaces of materials with different deformation properties exposed to cyclic loading leads to delamination and interfacial debonding.[7] Using reversible DA networks, multimaterial interfaces and components can be made more robust, as illustrated by the development of multimaterial healable soft grippers out of multiple DA elastomers.[26,34] The tunability of the mechanical properties and the compatibility of multiple DA networks integrated in a single part provide a large design freedom for future applications. Material models that are fitted onto these mechanical behaviors can be adopted in FEA simulations used to design or control (robotic) components. An example is presented by Ferrentino et al.,[46] in which constitutive material laws are fitted onto the hyperelastic behavior of a DPBM-FT5000-*r*0.5 network. This fitted neo-Hookean law is used to simulate and control a healable soft robotic actuator made from the DA network.

CONCLUSIONS

The wide range of properties of the synthesized and characterized DA networks described in this paper illustrates their potential for diverse applications, including soft robotics. This work presented the direct effects of the three network design parameters, DA concentration at 25 °C, functionality, and stoichiometry, on the macroscopic material properties. We made special efforts to independently change the network design parameters, while keeping the others constant, to investigate their effect on the thermomechanical and viscoelastic behavior, and on the reaction kinetics. Although not completely independent, the three network design parameters allow us to design and tune individually the mechanical properties, (de)gelation transition, and healing performance (Figure 1). This decoupling provides an interesting degree of freedom for designing networks that suit both manufacturing techniques and application requirements. As such, this work provides the key insights for designing intrinsic self-healing elastomers based on thermoreversible DA chemistries for future applications. Because of the large degree of freedom in changing the material properties independently, the authors are convinced that thermoreversible networks, and in particular reversible elastomers based on the Diels−Alder chemistry, will be increasingly used in healable soft robotics. The ability to heal damage will increase the lifetime of components, which, in combination with the recycling and reprocessing potential of these materials, paves the way to more sustainable products.

EXPERIMENTAL SECTION

Materials. Three diamines, Jeffamines D400, D2000, and D4000, which are poly (propylene oxide) bis(2-amino propyl ether), with repeated oxypropylene units in the backbone and average molar masses of 432, 1793, and 4546 g mol^{-1}, respectively, were used in this publication. Three triamines, Jeffamines T3000, T5000-1, and T5000-2 were used, having trifunctional polypropylene glycol backbones and average molar masses of 3240, 5712, and 6650 g mol^{-1}, respectively. D400, D4000, T3000, and T5000-2 were supplied by Huntsman (Belgium). D2000 and T5000-1 were supplied by Aurora Chemicals (China). The molar masses were determined using NMR in Supporting Information 3. Furfuryl glycidyl ether (FGE), with a purity of 95%, was purchased from Sage Chemicals (China) and stored in refrigerated conditions. 1,1′-(Methylenedi-4,1-phenylene)-bismaleimide (DPBM) with a purity of 95% was obtained from Sage Chemicals (China). Hydroquinone (1,4-benzenediol) was used as a radical inhibitor and was supplied by Sigma-Aldrich. Chloroform (stab./amylene) (minimum of 99.9%) was obtained from Biosolve Chimie. All chemicals were used as delivered. The chemical structure of these reagents is presented in Figure 17, as well as in Supporting Information 2.

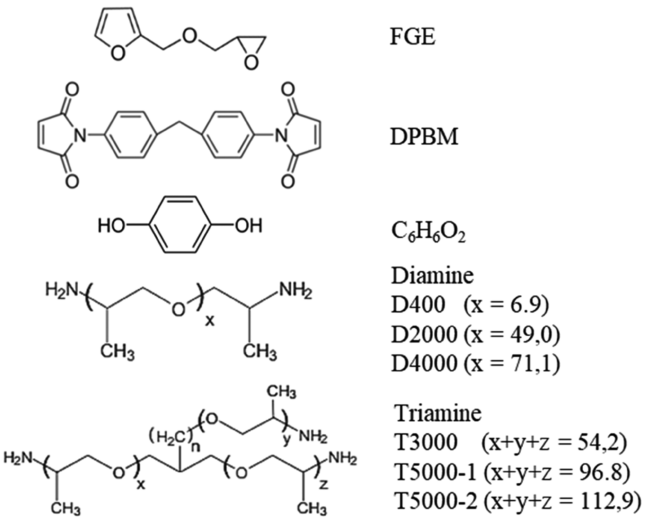

Figure 17. Reagents of the reversible DA networks, including furfuryl glycidyl ether (FGE), 1,1′-(methylenedi-4,1-phenylene)bismaleimide (DPBM), hydroquinone ($C_6H_6O_2$: 1,4-benzenediol), D400, D2000, and D4000 diamines and T3000, T5000-1, and T5000-2 triamines.

Synthesis. FGE is reacted with a stoichiometric amount of Jeffamine, yielding a furan-functionalized Jeffamine (FFJ) compound. This reaction was performed for a minimum of 7 days at 60 °C under continuous magnetic stirring, after which the reaction was completed for 4 days at 90 °C. To synthesize the network, FFJ, DPBM, and hydroquinone (5 wt % of DPBM) were dissolved in chloroform (20 wt %) and stirred using a magnetic stirrer for 24 h. The polymerization is performed through solvent casting. The chloroform is extracted through vacuum at room temperature for 24 h. As the reactant concentration increases by the evaporation of the solvent, the

https://doi.org/10.1021/acs.macromol.2c00434
Macromolecules 2022, 55, 5497−5513

network is gradually formed through DA crosslinking. A more detailed synthesis report can be found in Supporting Information 4. Synthesized network samples were stored at 25 °C.

DSC. Differential scanning calorimetry (DSC) was performed using a TA Instruments Discovery DSC. The DSC was equipped with a refrigerated cooling system (RCS) that allows cooling down to −90 °C. Nitrogen was used as a purge gas. The DA network samples (15−20 mg) were measured in TA Instruments Tzero pans with perforated Tzero hermetic lids to ensure an inert atmosphere above the sample. The DSC has a temperature accuracy of ±0.025 K.

Tensile Testing. Tensile testing with a fixed strain ramp of 1% s^{-1} until fracture was also performed on a TA Instruments DMA Q800 at ambient temperature, using 5 × 30 × 1 mm^3 samples and a gauge length of 7−8 mm. Engineering stresses and engineering strains are used to calculate the Young's modulus, fracture strain, and fracture stress.

DMA. Dynamic mechanical analysis (DMA) was performed on a TA Instruments DMA Q800 equipped with a liquid nitrogen cooling system (LNCS). 5 × 30 × 1 mm^3 samples were clamped with a gauge length of 15 mm in a tensile clamp setup. Oscillating strains with an amplitude of 0.2% and a frequency of 1 Hz were used to characterize the viscoelastic properties in the −80 to 100 °C temperature window, using a temperature ramp of 1 K min^{-1}. The DMA Q800 has a temperature accuracy of ±0.1 K.

Rheometry. Dynamic rheometry was performed on a TA Instruments Discovery Hybrid Rheometer DHR-2, equipped with an environmental test chamber (ETC) to control the temperature. Sample disks with a diameter of 14 mm and a thickness of 1 mm were placed between disposable aluminum parallel-plate geometries with a diameter of 14 mm. Samples were subjected to a stepwise temperature increase of 2 K after an isothermal of 10 min. More details on this temperature profile can be found in Supporting Information 5. At the end of each isothermal segment, the samples underwent a multifrequency test that subjects the samples to sinusoidal strains with a strain amplitude of 10% at frequencies of 10, 6.31, 3.98, 2.51, 1.58, and 1 Hz. The DHR-2 has a temperature accuracy of ±0.1 K.

■ ASSOCIATED CONTENT

Supporting Information

The Supporting Information is available free of charge at https://pubs.acs.org/doi/10.1021/acs.macromol.2c00434.

Determination of the kinetic parameters for the DPBM-FFJs systems (Supporting Information 1); chemical formulas of the reagents (Supporting Information 2); NMR spectra of Jeffamines (Supporting Information 3); synthesis of DPBM-FFJ networks (Supporting Information 4); and dynamic rheometry on DPBM-FFJ networks (Supporting Information 5) (PDF)

■ AUTHOR INFORMATION

Corresponding Author

Seppe Terryn − *Brubotics, Vrije Universiteit Brussel (VUB) and Imec, B-1050 Brussels, Belgium;* orcid.org/0000-0002-9213-4502; Email: Seppe.terryn@vub.be

Authors

Joost Brancart − *Physical Chemistry and Polymer Science (FYSC), VUB, B-1050 Brussels, Belgium;* orcid.org/0000-0002-1735-1515

Ellen Roels − *Brubotics, Vrije Universiteit Brussel (VUB) and Imec, B-1050 Brussels, Belgium*

Robrecht Verhelle − *Physical Chemistry and Polymer Science (FYSC), VUB, B-1050 Brussels, Belgium;* orcid.org/0000-0002-3700-5169

Ali Safaei − *Physical Chemistry and Polymer Science (FYSC), VUB, B-1050 Brussels, Belgium*

Audrey Cuvellier − *Physical Chemistry and Polymer Science (FYSC), VUB, B-1050 Brussels, Belgium*

Bram Vanderborght − *Brubotics, Vrije Universiteit Brussel (VUB) and Imec, B-1050 Brussels, Belgium*

Guy Van Assche − *Physical Chemistry and Polymer Science (FYSC), VUB, B-1050 Brussels, Belgium;* orcid.org/0000-0003-0452-6272

Complete contact information is available at: https://pubs.acs.org/10.1021/acs.macromol.2c00434

Notes

The authors declare no competing financial interest.

■ ACKNOWLEDGMENTS

This research was performed in relation to and funded by the EU FET Open RIA Project SHERO (828818), the EU Marie Curie ITN Project SMART (860108), and the FWO SBO Project AMSeR (G028218N). In addition, the authors gratefully acknowledge the Fonds Wetenschappelijk Onderzoek (FWO) for the personal grants to S.T. (1100416N), J.B. (12W4719N), A.C. (1S40617N), and E.R. (1S84120N).

■ REFERENCES

(1) Dahlke, J.; Zechel, S.; Hager, M. D.; Schubert, U. S. How to Design a Self-Healing Polymer: General Concepts of Dynamic Covalent Bonds and Their Application for Intrinsic Healable Materials. *Adv. Mater. Interfaces* **2018**, *5*, 1800051.

(2) Kuang, X.; Liu, G.; Dong, X.; Liu, X.; Xu, J.; Wang, D. Facile Fabrication of Fast Recyclable and Multiple Self-Healing Epoxy Materials through Diels-Alder Adduct Cross-Linker. *J. Polym. Sci., Part A: Polym. Chem.* **2015**, *53*, 2094−2103.

(3) Diels, O.; Kech, H. Synthesen in der Hydroaromatischen Reihe. XXIV; "Dien-Synthesen" Stickstoffhaltiger Heteroringe. *Justus Liebigs Ann. Chem.* **1935**, *519*, 140−146.

(4) Brancart, J.; Verhelle, R.; Mangialetto, J.; Van Assche, G. Coupling the Microscopic Healing Behaviour of Coatings to the Thermoreversible Diels−Alder Network Formation. *Coatings* **2019**, *9*, 13.

(5) Vauthier, M.; Jierry, L.; Oliveira, J. C.; Hassouna, L.; Roucoules, V.; Bally-Le Gall, F. Interfacial Thermoreversible Chemistry on Functional Coatings: A Focus on the Diels−Alder Reaction. *Adv. Funct. Mater.* **2019**, *29*, 1806765.

(6) Brancart, J.; Scheltjens, G.; Muselle, T.; Van Mele, B.; Terryn, H.; Van Assche, G. Atomic Force Microscopy Based Study of Self-Healing Coatings Based on Reversible Polymer Network Systems. *J. Intell. Mater. Syst. Struct.* **2014**, *25*, 40−46.

(7) Terryn, S.; Langenbach, J.; Roels, E.; Brancart, J.; Thuruthel, T. G.; Safaei, A.; Ferrentino, P.; Sebastian, T.; Bakkali, C.; Norvez, S.; Iida, F.; Bosman, A. W.; Tournilhac, F.; Clemens, F.; Van Assche, G.; Vanderborght, B.; et al. A Review on Self-Healing Polymers for Soft Robotics. *Mater. Today* **2021**, *47*, 187−205.

(8) Yang, K.; Grant, J. C.; Lamey, P.; Joshi-imre, A.; Lund, B. R.; Smaldone, R. A.; Voit, W. Diels−Alder Reversible Thermoset 3D Printing Isotropic Thermoset Polymers via Fused Filament Fabrication. *Adv. Funct. Mater.* **2017**, *27*, No. 1700318.

(9) Rus, D.; Tolley, M. T. Design, Fabrication and Control of Soft Robots. *Nature* **2015**, *521*, 467−475.

(10) Shintake, J.; Cacucciolo, V.; Floreano, D.; Shea, H. Soft Robotic Grippers. *Adv. Mater.* **2018**, *30*, No. 1707035.

(11) Wang, Z.; Torigoe, Y.; Hirai, S. A Prestressed Soft Gripper: Design, Modeling, Fabrication, and Tests for Food Handling. *IEEE Rob. Autom. Lett.* **2017**, *2*, 1909−1916.

(12) Cheng, N.; Amend, J.; Farrell, T.; Latour, D.; Martinez, C.; Johansson, J.; McNicoll, A.; Wartenberg, M.; Naseef, S.; Hanson, W.; Culley, W. Prosthetic Jamming Terminal Device: A Case Study of Untethered Soft Robotics. *Soft Rob.* **2016**, *3*, 205−212.

(13) Saldien, J.; Goris, K.; Vanderborght, B.; Vanderfaeillie, J.; Lefeber, D. Expressing Emotions with the Social Robot Probo. *Int. J. Soc. Rob.* **2010**, *2*, 377−389.
(14) Runciman, M.; Darzi, A.; Mylonas, G. P. Soft Robotics in Minimally Invasive Surgery. *Soft Rob.* **2019**, *6*, 423−443.
(15) Markvicka, E. J.; Bartlett, M. D.; Huang, X.; Majidi, C. An Autonomously Electrically Self-Healing Liquid Metal-Elastomer Composite for Robust Soft-Matter Robotics and Electronics. *Nat. Mater.* **2018**, *17*, 618−624.
(16) Case, J. C.; White, E. L.; Kramer, R. K. Soft Material Characterization for Robotic Applications. *Soft Rob.* **2015**, *2*, 80−87.
(17) Wallin, T. J.; Pikul, J. H.; Bodkhe, S.; Peele, B. N.; Mac Murray, B. C.; Therriault, D.; McEnerney, B. W.; Dillon, R. P.; Giannelis, E. P.; Shepherd, R. F. Click Chemistry Stereolithography for Soft Robots That Self-Heal. *J. Mater. Chem. B* **2017**, *5*, 6249−6255.
(18) Pena-Francesch, A.; Jung, H.; Demirel, M. C.; Sitti, M. Biosynthetic Self-Healing Materials for Soft Machines. *Nat. Mater.* **2020**, *19*, 1230−1235.
(19) Yu, K.; Xin, A.; Du, H.; Li, Y.; Wang, Q. Additive Manufacturing of Self-Healing Elastomers. *NPG Asia Mater.* **2019**, *11*, 7.
(20) Terryn, S.; Brancart, J.; Lefeber, D.; Van Assche, G.; Vanderborght, B. Self-Healing Soft Pneumatic Robots. *Sci. Rob.* **2017**, *2*, eaan4268.
(21) Guimarães, C. F.; Gasperini, L.; Marques, A. P.; Reis, R. L. The Stiffness of Living Tissues and Its Implications for Tissue Engineering. *Nat. Rev. Mater.* **2020**, *5*, 351−370.
(22) Hughes, J. A. E.; Maiolino, P.; Iida, F. An Anthropomorphic Soft Skeleton Hand Exploiting Conditional Models for Piano Playing. *Sci. Rob.* **2018**, *3*, eaau3098.
(23) Ding, L.; Dai, N.; Mu, X.; Xie, S.; Fan, X.; Li, D.; Cheng, X. Design of Soft Multi-Material Pneumatic Actuators Based on Principal Strain Field. *Mater. Des.* **2019**, *182*, No. 108000.
(24) Terryn, S.; Mathijssen, G.; Brancart, J.; Lefeber, D.; Van Assche, G.; Vanderborght, B. Development of a Self-Healing Soft Pneumatic Actuator: A First Concept. *Bioinspiration Biomimetics* **2015**, *10*, No. 046007.
(25) Orozco, F.; Li, J.; Ezekiel, U.; Niyazov, Z.; Floyd, L.; Lima, G. M. R.; Winkelman, J. G. M.; Moreno-Villoslada, I.; Picchioni, F.; Bose, R. K. Diels−Alder-Based Thermo-Reversibly Crosslinked Polymers: Interplay of Crosslinking Density, Network Mobility, Kinetics and Stereoisomerism. *Eur. Polym. J.* **2020**, *135*, No. 109882.
(26) Terryn, S.; Roels, E.; Brancart, J.; Van Assche, G.; Vanderborght, B. Self-Healing and High Interfacial Strength in Multi-Material Soft Pneumatic Robots via Reversible Diels−Alder Bonds. *Actuators* **2020**, *9*, 34.
(27) Zeng, C.; Seino, H.; Ren, J.; Hatanaka, K.; Yoshie, N. Self-Healing Bio-Based Furan Polymers Cross-Linked with Various Bis-Maleimides. *Macromolecules* **2013**, *54*, 5351−5357.
(28) Safaei, A.; Terryn, S.; Vanderborght, B.; Van Assche, G.; Brancart, J. The Influence of the Furan and Maleimide Stoichiometry on the Thermoreversible Diels−Alder Network Polymerization. *Polymers* **2021**, *13*, 2522.
(29) Winter, H. H. Can the Gel Point of a Cross-Linking Polymer Be Detected. *Polym. Eng. Sci.* **1987**, *27*, 1698−1702.
(30) Li, X.; Becquart, F.; Taha, M.; Majesté, J.-C.; Chen, J.; Zhang, S.; Mignard, N. Tuning the Thermoreversible Temperature Domain of PTMC-Based Networks with Thermosensitive Links Concentration. *Soft Matter* **2020**, *16*, 2815−2828.
(31) Roels, E.; Terryn, S.; Brancart, J.; Verhelle, R.; Van Assche, G.; Vanderborght, B. Additive Manufacturing for Self-Healing Soft Robots. *Soft Rob.* **2020**, *7*, 711−723.
(32) Cuvellier, A.; Verhelle, R.; Brancart, J.; Vanderborght, B.; Assche, G.; Van; Rahier, H. Polymer Chemistry The Influence of Stereochemistry on the Reactivity of the Diels−Alder Cycloaddition. *Polym. Chem.* **2019**, *10*, 473−485.
(33) Terryn, S.; Brancart, J.; Roels, E.; Van Assche, G.; Vanderborght, B. Room-Temperature Self-Healing in Soft Pneumatic Robotics. *IEEE Rob. Autom. Mag.* **2020**, *27*, 44−55.
(34) Roels, E.; Terryn, S.; Brancart, J.; Van Assche, G.; Vanderborght, B. A Multi-Material Self-Healing Soft Gripper. In *IEEE International Conference on Soft Robotics (RoboSoft)*; IEEE, 2019; pp 316−321.
(35) Roels, E.; Terryn, S.; Brancart, J.; Verhelle, R.; Van Assche, G.; Vanderborght, B. Additive Manufacturing for Self-Healing Soft Robots. *Soft Rob.* **2020**, *7*, 711.
(36) Zhou, Q.; Gardea, F.; Sang, Z.; Lee, S.; Pharr, M.; Sukhishvili, S. A. A Tailorable Family of Elastomeric-to-Rigid, 3D Printable, Interbonding Polymer Networks. *Adv. Funct. Mater.* **2020**, *30*, 2002374.
(37) Froidevaux, V.; Borne, M.; Laborbe, E.; Auvergne, R.; Gandini, A.; Boutevin, B. Study of the Diels−Alder and Retro-Diels−Alder Reaction between Furan Derivatives and Maleimide for the Creation of New Materials. *RSC Adv.* **2015**, *5*, 37742−37754.
(38) Scheltjens, G.; Diaz, M. M.; Brancart, J.; Van Assche, G.; Van Mele, B. A Self-Healing Polymer Network Based on Reversible Covalent Bonding. *React. Funct. Polym.* **2013**, *73*, 413−420.
(39) Polgar, L. M.; Van Duin, M.; Broekhuis, A. A.; Picchioni, F. Use of Diels−Alder Chemistry for Thermoreversible Cross-Linking of Rubbers: The next Step toward Recycling of Rubber Products? *Macromolecules* **2015**, *48*, 7096−7105.
(40) Terryn, S.; Mathijssen, G.; Brancart, J.; Verstraten, T.; Van Assche, G.; Vanderborght, B. Toward Self-Healing Actuators: A Preliminary Concept. *IEEE Trans. Rob.* **2016**, *32*, 736−743.
(41) Flory, J. Molecular Size Distribution in Three Dimensional Polymers. I. Gelation. *J. Am. Chem. Soc.* **1941**, *63*, 3083−3090.
(42) Stockmayer, W. H. Theory of Molecular Size Distribution and Gel Formation in Branched Polymers II. General Cross Linking. *J. Chem. Phys.* **1944**, *12*, 125−131.
(43) Ehrhardt, D.; Mangialetto, J.; Bertouille, J.; Van Durme, K.; Van Mele, B.; Van den Brande, N. Self-Healing in Mobility-Restricted Conditions Maintaining Mechanical Robustness: Furan−Maleimide Diels−Alder Cycloadditions in Polymer Networks for Ambient Applications. *Polymers* **2020**, *12*, 2543.
(44) Wang, S.; Urban, M. W. Self-Healing Polymers. *Nat. Rev. Mater.* **2020**, *5*, 562−583.
(45) Cully, A.; Clune, J.; Tarapore, D.; Mouret, J. B. Robots That Can Adapt like Animals. *Nature* **2015**, *521*, 503−507.
(46) Ferrentino, P.; Tabrizian, S. K.; Van Assche, G.; Vanderborght, B.; Terryn, S. FEA Based Inverse Kinematic Control on Hyper-elasticmaterial Characterization of Self Healing Soft Robots. *IEEE Rob. Autom. Lett.* **2021**, DOI: 10.1109/MRA.2021.3132803.

https://doi.org/10.1021/acs.macromol.2c00434
Macromolecules 2022, 55, 5497−5513